On the Behaviour of Sea-Salt Based Batteries

by

Davey Sang Jae Kouwenberg

A Masters Thesis

Student number:	4192540
Thesis duration:	November 2021 – June 2022
Supervisor:	Dr. ir. L.M. Ramírez Elizondo
Advisor:	J.J. Alpízar Castillo
Thesis committee:	Prof. Dr. P. Bauer
	Prof. Dr. ir. A.H.M. Smets
	Dr. ir. L.M. Ramírez Elizondo

FACULTY OF ELECTRICAL ENGINEERING, MATHEMATICS AND COMPUTER SCIENCE

SUSTAINABLE ENERGY TECHNOLOGY

Abstract

The slow but ever-moving energy transition is slowly transforming the energy system from a fully controllable system on the generation side, to one that is dependent on the fickle nature of daily weather and seasonal patterns. This new energy system requires a buffer act as a mediator between varying generation of power, and varying consumption of power over time. Batteries are one of the main tools to provide flexibility in the system, but environmental and economical factors pose a significant problem. New types of batteries that do not rely on rare earth metals and organic solvents, but instead use water and more common ions could be a cost-effective and environmentally safe way to provide energy storage the future.

A sea-salt battery, designed on Dutch soil, promises to do just that. By using low-cost components and easily obtained materials, it aims to provide a low-cost environmentally friendly method to store electricity. This thesis aims to provide some insight in the performance of this battery. However, the exact composition is unclear, which severely hampers the analysis.

Several data sets, provided by the producer of the battery, were analysed to find trends and possible consistencies and pitfalls. One battery and several cells were also provided to perform in-house testing. A new metric was introduced to quantify the behaviour of the battery, analogous to the Maximum Power Point found in photovoltaics. The analysis of the data sets, and several charge/discharge cycle measurements on both the battery and the separate cells, revealed that while the measured voltage behaviour of the battery is consistent with the data sets, the efficiencies obtain through the in-house measurements do not correspond to the values found in the data sets. Furthermore, a comparison between the battery and the separate cells seems to indicate that one of the cells that constitute the battery may be faulty.

Some modelling was done, using the Distribution Buffer-model, to evaluate whether the battery's behaviour was consistent enough for future modelling. It was found that while fitting the model yielded a wide range of values for each of the constants, the model itself still yielded reasonable results in terms of energy capacity predictions.

In conclusion, the sea-salt battery, while promising, still has several hurdles to overcome in terms of performance and reliability. More insight into the internal composition is required to any further analysis, including determining the full capacity of the battery, and determining best practices for operation.

Acknowledgements

When I started this Masters program in 2019, I dove into it head first, with the goal to gain the knowledge and skills to 'save the world'. Climate change scares me profoundly, and I want to do whatever I can to stop it. No one could have imagined, however, that just one year later, the whole world would shut down. Just like many others, it had a large effect on my mental well-being.

It is hard to overstate how hard this whole process has been for me. From having to give up studying abroad, to the massive failure that was JIP for me, I found it incredibly hard to stay motivated through the second and now third year of my Masters. The fact that I managed to (hopefully) get it across the finish line is, at least to me, close to a miracle.

That is why I would first and foremost like to thank my supervisor and advisor, Laura and Joel. I want to thank them for their infinite patience with me. They have showed kindness, pragmatism and understanding when I needed it most, invested much of their time and energy in me, and somehow found time in their crazy schedules to help me whenever I asked for it. I most certainly would not have gotten through this without your support.

I would also like to thank my parents, who have freely given so much without expecting anything in return, my wonderful girlfriend Paulina for never doubting me for a second and supporting me in quite literally everything I do. I love you dearly and I cannot wait to see you this Christmas. Ivan, Mohamed and Maria, you are all absolutely hilarious and some of the smartest people I know, next time we will have to meet somewhere in France! Big thanks to Brendan, Vyshali, Nireeksha and Florien as well, JIP may have ended in disaster but it was a pleasure going through it with you. Thank to Bada, Annechien, Ricardo & co., Hooghe Clout, B37, the Coveteers, and any other friends I may have forgotten for keeping my spirits up in a million different ways.

So, what is next? I have no idea, but I am sure it will be something to sink my teeth into. And if it is as chewy as this thesis, at least I know I can bite through it.

Davey Sang Jae Kouwenberg
Amsterdam, November 2022

Contents

Abstract ii

Acknowledgements iv

1 Introduction 1
- 1.1 Motivation . . . 1
  - 1.1.1 Climate Change Action . . . 1
  - 1.1.2 Energy Distribution . . . 1
  - 1.1.3 Microgrids . . . 2
  - 1.1.4 Energy Storage . . . 3
- 1.2 Sea-Salt Battery . . . 3
- 1.3 Problem Statement . . . 7
- 1.4 Objective . . . 8
- 1.5 Research Questions . . . 8

2 Literature Review 9
- 2.1 Common battery types . . . 9
  - 2.1.1 Lithium-ion . . . 9
  - 2.1.2 Lead-acid . . . 10
  - 2.1.3 Nickel Cadmium/Metal Hydride . . . 11
- 2.2 Sea Salt Batteries . . . 12
- 2.3 DiBu-Model . . . 16
- 2.4 Maximum Power Point Analogy To Voltage Time . . . 18

3 Methodology 20
- 3.1 Data Analysis . . . 20
- 3.2 Equipment & Materials . . . 20
- 3.3 Battery Cycling . . . 20
  - 3.3.1 Constant Current . . . 20
  - 3.3.2 Constant Voltage . . . 23
- 3.4 MVTP Calculations . . . 23
- 3.5 Modelling . . . 23
  - 3.5.1 DiBu-Model . . . 25

4 Dr. Ten Data Set Analysis 27
- 4.1 General trends . . . 27
  - 4.1.1 Voltage Decay & Recovery . . . 31
  - 4.1.2 Voltage-Time . . . 31
- 4.2 Inconsistencies . . . 32

5 In-House Measurement Results & Discussion 36
- 5.1 General Trends . . . 36
- 5.2 Voltage-Time . . . 38
- 5.3 Capacity & Efficiency . . . 39
- 5.4 Constant Voltage Cycling . . . 40

5.5 Voltage-Limited Constant Current Cycling 42
5.6 Single Cell Measurements 43
5.7 Structural Integrity 45
5.8 Modelling 47

6 Conclusion **54**
6.1 Research Questions 54
6.2 Recommendations 55

1 Introduction

This Chapter will provide a general overview and background of this project. Section 1.1 will detail the motivation of this project. Section 1.2 expands on the battery that is studied in this work. Lastly, Sections 1.3, 1.4 and 1.5 will give the problem statement, the objective of this work, and its research questions.

1.1 Motivation

Ever since the discovery of fire, humanity has been slowly releasing more and more greenhouse gasses into the atmosphere. This has exponentially accelerated since the industrial revolution; the widespread usage of coal and oil to shape and power modern society has lead to a slow but inevitable rise in global average temperatures and associated changes in climate. Measurements on global temperatures have shown a 1.04°C increase since pre-industrial times, with a average increase of 0.14°C per decade since 1981 [1].

1.1.1 Climate Change Action

In response, several international climate accords have been signed; the Earth Summit saw the signing of the Rio Declaration in 1992 [2], followed by the Kyoto Protocol in 1997 [3]. The most recent Paris Agreement was signed in 2016 by a record 197 signatories, striving to reduce greenhouse gas emissions by 50% by 2030, and to limit the global temperature rise to 2°C above pre-industrial levels. Each signatory would be required to set its own targets and roadmap to achieve these targets, the accumulated effect of which should reach the Agreement's overall goals.

While these accords and agreements have had little direct impact on the total amount of emissions thus far, it has had a significant knock-on effect on the research and development of renewable energy sources via subsidies, emission taxes and other schemes. In the Netherlands, a combination the European Emission Trading Scheme [4] and subsidies for renewable energy and energy-saving measures [5] have made it increasingly attractive from an economical perspective for both businesses and individuals to dive into renewable energy. Stricter building codes have also lead to a gradual moving away from gas, with no new permits being handed out to connect newly built homes to the gas network [6].

1.1.2 Energy Distribution

The effects of these measures are clearly visible in the amount of installed capacity for renewable energy sources; according to CBS (Centraal Bureau voor de Statistiek), installed solar energy capacity has gone from 90 MW in 2010, to 14.4 GW in 2021. Likewise, installed wind energy capacity has also increased significantly (albeit not as rapidly), from 2.3 GW in 2010, to 7.72 GW in 2020, with several large scale wind farms being planned in the North Sea [7][8]. The difference in number of installed installations does stand out; while wind energy only features 2,865 installations as of 2021, solar energy boasts over 1.7 million installations, indicating a potentially sizeable contribution of individual homeowners and micro-installations.

This has had an unfortunate side effect for our grid; coupled with the increased electrification of households, and the constant addition of data centres and supermarkets throughout the country, both the transmission and distribution grids are quickly reaching maximum capacity. As of June 9th 2022, almost half of the distribution network managed by Liander has no spare capacity [9]. Mid July, Tennet announced that no new large scale users could be connected to the transmission grid in provinces Noord Brabant and Limburg [10]. Additional capacity would solve this problem in the short term, but in the long term, a different solution would be needed.

1.1.3 Microgrids

One of the proposed methods to increase grid flexibility without a forced overbuilding of capacity is to reshape the energy grid to form microgrids. These are described as localized grids, containing a set of loads, energy storage devices, and one or more modes of energy generation [11]. They are capable of operating while connected to the grid (also known as connected mode), as well as autonomously (islanded mode) in case the main grid is somehow compromised or for economical or logistical reasons [12]. To ensure proper operation in islanded mode, communication between all devices in the grid and a centralized control system is required; the control system ensures that the grid is maintained within safe operating levels. They can vary from just a single household with PV systems and a battery in the garage, to a an entire university campus.

Microgrids solve several problems at once. First and foremost, by putting generation closer to the loads, the transmission networks linking these microgrids in general could require less capacity, as most of the demand can be fulfilled by nearby sources. This also increases overall efficiency; shorter cables mean less power loss, as well as decreased reactive power needs, depending on whether the microgrid operates using AC or DC voltage.

Microgrids are also much more robust than conventional networks [11]. The clearest benefactors of this characteristic are institutions that require power at all times, like hospitals. Instead of being reliant on the main grid, with diesel generators as a back-up, the focus could shift to having access to their own source of power at all times, only using the main grid when in-house generation falls short. Small-scale examples can already be found across the globe; individual households that have invested in PV panels and a moderately sized battery system can encounter multiple days where zero exchange with the grid is necessary, essentially becoming self-sufficient.

1.1.4 Energy Storage

One of the biggest challenges of any type of grid is maintaining the balance between power production and consumption. Overproduction can cause damage to valuable infrastructure and devices that are connected to the grid, while overconsumption can cause local or even total black-outs. Demand rises and falls throughout the day, and currently the balance is maintained by ramping up and down energy generators to match this demand. This is usually done by gas-powered generators, as they can ramp up and down rapidly within short time frames (on the order of several minutes). Having a fully controllable generation side means that the consumer has no need to keep in mind the grid's limitations; it is up to the energy generator to bow to the wishes of the consumer side.

When adding renewable energy into the mix, things get more complicated; solar and wind energy generation are completely dependent on the weather and seasonal conditions, and can vary strongly throughout the day and from season to season. Adding to this the constantly changing power demand creates a wildly fluctuating situation, going from energy deficiency to surplus within a matter of hours or even minutes, as well as longer term mismatches as demand increases during winter while renewable energy generation falls, and vice versa during summer.

With energy mismatches at every level (from seconds to months), it is clear energy storage systems are needed to maintain balance on the grid. They enable the grid operator to absorb and store energy when supply outruns demand, and release it when demand outruns supply, as well as use the available energy to ensure power quality. in the case of microgrids, energy storage systems can provide ancillary services to neighbouring microgrids, and more importantly, enable the microgrid to operate in islanded mode for extended periods of time. This can be done on any time scale, depending on the technology; fuel cells and potential energy storage devices can solve mismatches on a seasonal scale, while super-capacitors and batteries can balance out the grid from second to second and provide reactive power, with batteries potentially making up differences over the time span of a month. In short, it is these energy storage devices that enable microgrids to operate autonomously for extended periods of time, if not indefinitely. This body of work will focus on the analysis of a specific battery.

1.2 Sea-Salt Battery

The battery in question is based on zinc-halide and sodium-halide interactions. Prior work was done by Homan [13] in developing and characterizing this battery. The following Section will provide a summary of his work, along with some observations about said work.

Chapter 2 of Homan's PhD thesis analyses the performance of the developed sea-salt battery, applies a model he developed to predict its State of Charge, and sees the battery used for peak shaving in a real-life situation.

Homan expands on the main design philosophy behind the battery. The battery was to be *environmentally responsible*, *durable* and *affordable.* The first was addressed by only using chemicals that have the lowest GHS hazard rating [13]. The full list is shown in Table 1. However, note that the last two entries, 'Amine complexes' and 'Organic surfactants' are not specified, as these are 'company confidential'. Furthermore, Homan mentions that 'due to confidentiality, no specific concentrations of the various components of the electrolyte are given' [13]. The exact half reactions are also a company secret.

Table 1: Components used in the sea-salt battery and their GHS hazard classification [13].

Component	**Role**	**Hazard classification**
Electrode		
Treated graphite plate	Anode/Cathode	None
Treate graphite felt	Anode/Cathode	None
Electrolyte		
Water	Solvent	None
NaCl (aq)	Main component	None
$ZnCl_2$ (aq)	Main component	Warning, Corrosive, Danger to aquatic life
NaBr (aq)	Main component	None
$ZnBr_2$ (aq)	Main component	Warning, Corrosive, Danger to aquatic life
$AlCl_3$ (aq)	Catalyst	Corrosive
$MgBr_2$ (aq)	Dendrite prevention agent	Warning
Amine complexes	Stabilizer	n/a
Organic surfactants	Stabilier	n/a

The affordability of the battery's design was addressed by using as many low-cost materials as possible. To that end, indivudual cells were connected with graphite rods instead of more expensive copper wire, and a custom casing was developed that eliminated the needs of a filler cap for the electrolyte. The electrodes and electrolyte are all abundant chemicals, making them cheaper to acquire [13].

Repeated cycling measurements were done to determine the durability. A battery prototype, rated at 50 mAh, was cycled at 50 mA over 1400 cycles, with a lower limit of 0.7 V. Figure 1 shows the first and final 10 cycles. Between those 1400 cycles, Homan reported a drop in Coulombic efficiency from 94% to 72.4%, and a drop in energy efficiency from 65.5% to 31.3% [13]. Homan states that the battery has not yet failed, as the power efficiency is still above 50% of the original value, and the Coulombic efficiency is still above 75% of the original value, outperforming lead-acid batteries, while being slightly outperformed by lithium-ion batteries [13]. Note that the prototype, while similar to the final battery design, does not contain the amine complexes or organic surfactants.

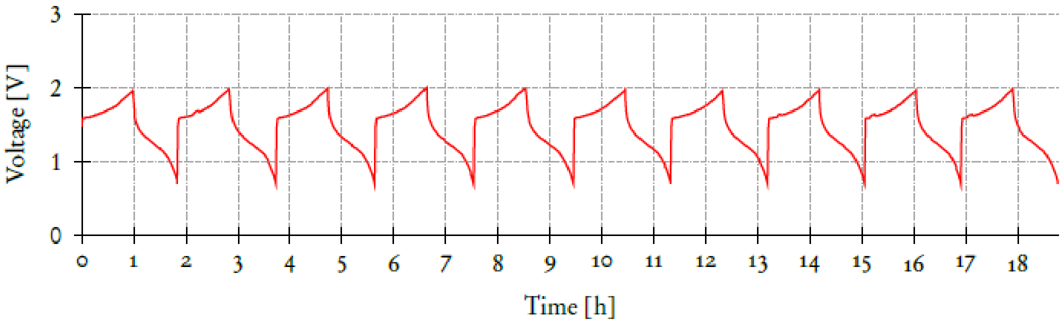

(a) First 10 cycles of the stress test

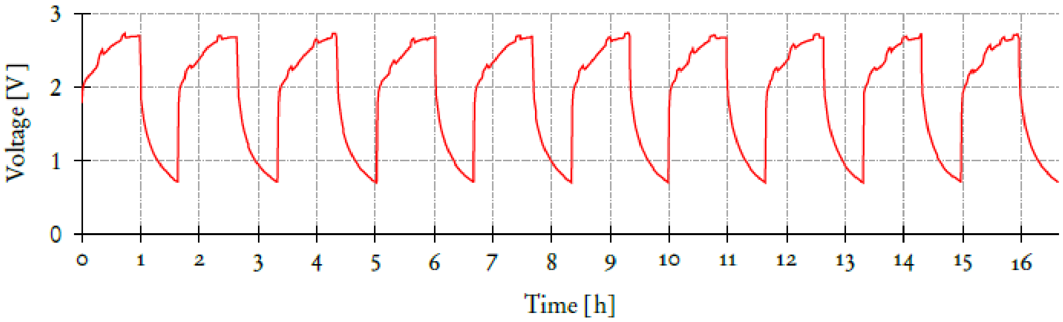

(b) Final 10 cycles of the stress test. The charge voltage has strongly increased, as has the overall shape of each cycle.

Figure 1: (a) A comparison between the first cycles and final cycles of a sea-salt battery [13]. The behaviour of the battery has changed significantly, as the charge voltage has increased, and the discharge voltage resembles part of an exponential decay.

Figures 2a and 2b show the charge and discharge behaviour of the final design of the sea-salt battery. The voltage remains a constant 1.8 V while charging, despite charging at constant current. When discharging, the voltage follows a behaviour similar to conventional battery technologies. The discharge was stopped at 1.2 V. These results do seem to conflict with Figure 2c, which shows two consecutive charge/discharge cycles. While the discharge phase seems largely similar, the charge phase sees a slow yet clear and consistent near-linear increase in voltage over time. Regardless, the behaviour during the charging phase means that using *off-the-shelf* equipment to control the battery becomes highly problematic, as existing equipment generally uses voltage readings to determine the State of Charge [13].

Using a model of his own design, Homan successfully modeled the State of Charge of the sea-salt battery over a period of 18 hours, with a slight alteration to the model to accommodate for the deviating behaviour during the charge phase. The average difference between measured State of Charge and modelled State of Charge was around 2% [13]. These results indicate that the battery operates consistently enough in combination with the model that viable work can be done. However, there is no mention on how the State of Charge was monitored when per-

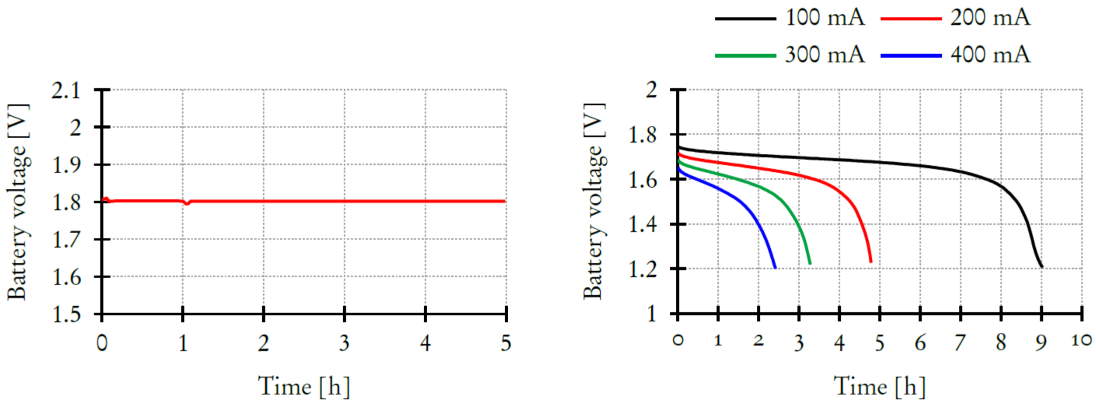

(a) Charge graph for the final design of the sea-salt battery

(b) Discharge graph of the sea-salt battery at different applied currents.

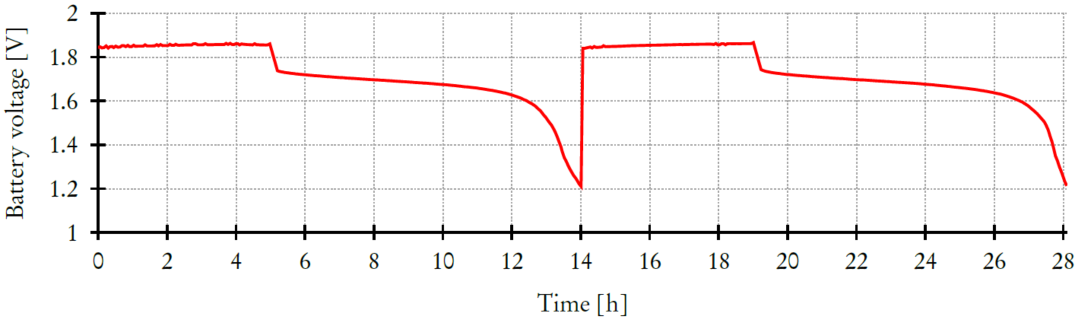

(c) Two consecutive charge/discharge cycles. The charge phase differs slightly from Figure 2a, with the voltage slowly increasing over time.

Figure 2: Different cycling graphs for the sea-salt battery. (a) A single charge phase at 100 mA, (b) 4 discharge responses at varying applied currents, (c) two consecutive constant current charge/discharge cycles at 250 mA charge, 100 mA discharge currents.

forming the comparative measurements. The model itself and its relation to this body of work will be further detailed in Chapters 2.3 and 3.5.1.

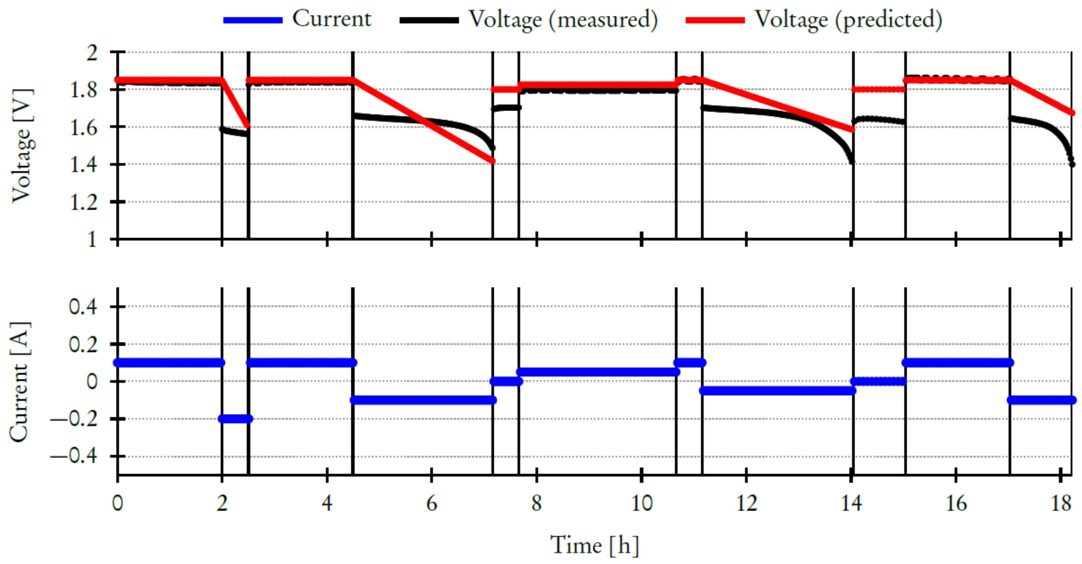

(a) The voltage predictions of Homan's model seem to function well when charging, but deviate more strongly when discharging.

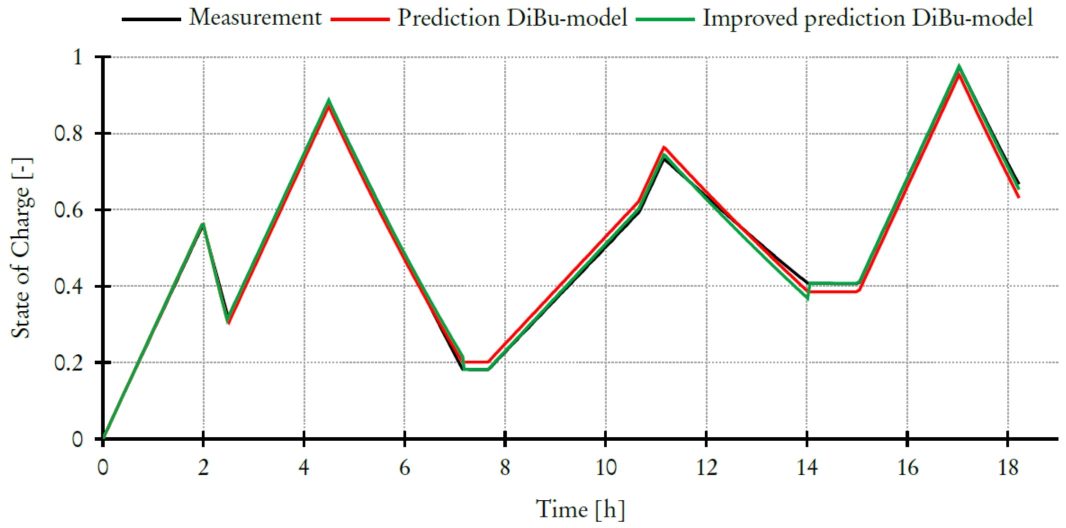

(b) Homan's model was able to predict the State of Charge to a high level of accuracy.

Figure 3: Results from the application of Homan's model on the sea-salt battery [13]. While there is a clear deviation in the behaviour of the voltage, the State of Charge prediction seems to be accurate.

1.3 Problem Statement

While Homan has done preliminary work on characterising the sea-salt battery, there is no data sheet available, nor has any external laboratory or institute had the opportunity to do any analysis of available data or any in-house testing of the battery. Inconsistencies in Homan's data and lack of detailed measurements performed on a universal platform cast doubt over the capabilities and capacity of the sea-salt battery.

1.4 Objective

The objective of this thesis is to quantify the behaviour and performance of the sea-salt battery, and identify its potential for residential applications.

1.5 Research Questions

- What are the energy and charge capacity of the sea-salt based battery?
- What is the round-trip efficiency of the battery?
- How do different cycling parameters influence performance?
- What are the set points to be used for safely charging and discharging the battery?
- Does the battery operate consistently enough to create a usable model?

2 Literature Review

This Chapter gives the necessary background and context to understand the results and analyses. Section 2.1 will go over the technical aspects of some of the most common types of batteries. Section 2.2 gives an overview of some sea-salt batteries currently under development. Section 2.3 will expands on the background of the DiBu-model, designed by Homan [13]. Finally, Section 2.4 introduces the concept of Maximum Voltage Time Point, which will be used to quantify some of the behaviour of the sea-salt battery.

2.1 Common battery types

In the rechargeable battery space, three of the most common types are lithium-ion, lead-acid, and nickel metal-hydride batteries. This section gives an abbreviated description of each type, with some performance metrics and general behaviour.

2.1.1 Lithium-ion

Lithium-ion batteries are the most common battery type in today's society. They boast high specific energy, specific power and efficiency, which makes them a prime candidate for a wide variety of applications, from portable electronics to large-scale power storage [14]. They are also lighter than other battery technologies, and have a very low self-discharge. They are, however, expensive to produce, due to the scarcity of the required materials.

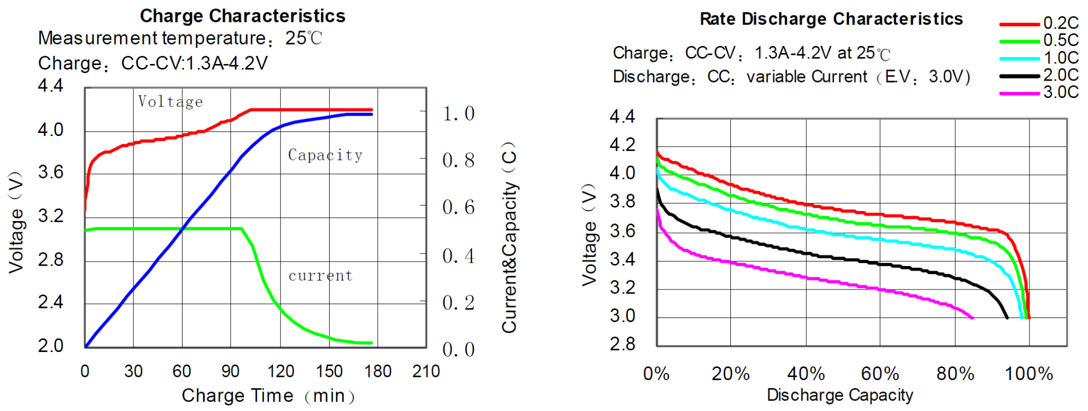

(a) The charge curve for a commercial lithium-ion battery. Halfway through the charge time the method changes from constant current to constant voltage, to protect the battery.

(b) Discharge curves at different C rates. Only towards higher discharge capacities does the voltage drop sharply.

Figure 4: Charge and discharge curves for a commercial lithium-ion battery [15].

Li-ion batteries are typically constructed using a carbon-based anode and a transition metal oxide cathode, with an organic solvent or polymer as electrolyte.

The choice of transition metal for the cathode determines most of the characteristics of the battery. Typical Li-ion cells have an OCV of either 3.6 V or 4.2 V. They have an average energy efficiency of over 95%. The organic solvent constitutes a serious safety risk, as damage to or improper use of the battery can cause the battery to combust. Polymer-based electrolytes have been introduced to mitigate this hazard. The polymer electrolyte does introduce structural limitations, as they cannot be produced as thin as liquid electrolytes, limiting the amount of contact surface area with the electrode, which decreases the maximum output power. Despite this drawback, lithium-polymer batteries are seeing slowly increasing use in portable electronics. A lack of standardization in both the internal chemistry and construction makes them hard to recycle, with less than 10% of all Li-ion batteries being recycled in Europe as of 2019 [16]. Lithium-ion batteries can last up to 1000 cycles, depending on the materials used, operating conditions and charge protocols [17][18]. Figure 4 shows charge and discharge cycles for a commercial lithium-ion battery [15], at different discharging rates.

2.1.2 Lead-acid

Lead acid batteries have been around for over a century, both used in deep-cycle situations (e.g. boats, campers), as well as situations in which short bursts of power are required, like igniting the engine of a car. Lead-acid batteries are marked by high toxicity and acidity, and low specific energy, but high specific power, though this is dependent on the overall construction [14].

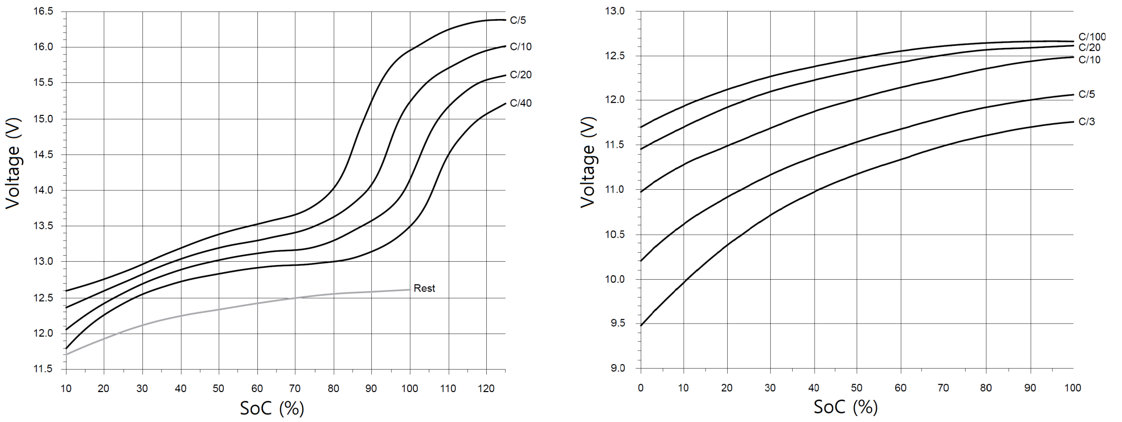

(a) Typical lead-acid battery voltage at different charge rates [19]. Note the secondary increase in voltage towards higher SoC levels.

(b) Typical lead-acid battery voltage at different discharge rates [19]. The voltage decreases strongly with increased discharge rates.

Figure 5: Typical charge and discharge curves for a commercial lead-acid battery.

A single cell has an OCV of around 2 V. Most commercial lead-acid batteries are designed to deliver 12 V. They generally operate at 85% Coulombic efficiency and around 70% energy efficiency, though this strongly depends on the applied currents when discharging; both the discharge voltage and available capacity significantly decrease at higher discharge rates [20][19]. The typical lifespan of modern lead-acid batteries in commercial applications is between 2000 and 5000 cycles. Despite the high toxicity and acidity of the battery, standardized internal chemistry and construction makes lead-acid batteries easy to recycle. As of 2013, all lead production in the US currently comes from recycling lead [21]. Figure 5 shows typical charge and discharge curves for a lead-acid battery.

2.1.3 Nickel Cadmium/Metal Hydride

Nickelcadmium (NiCd) batteries have been around since the early 20th century, with nickel metal hydride (NiMH) batteries following in the late 1980s to early 1990s. NiMH are currently more in favour due to higher energy densities, and absence of the memory effect (partial discharge leading to a reduction in capacity). They are also less harmful to the environment, replacing highly toxic cadmium with less toxic transition metals [14].

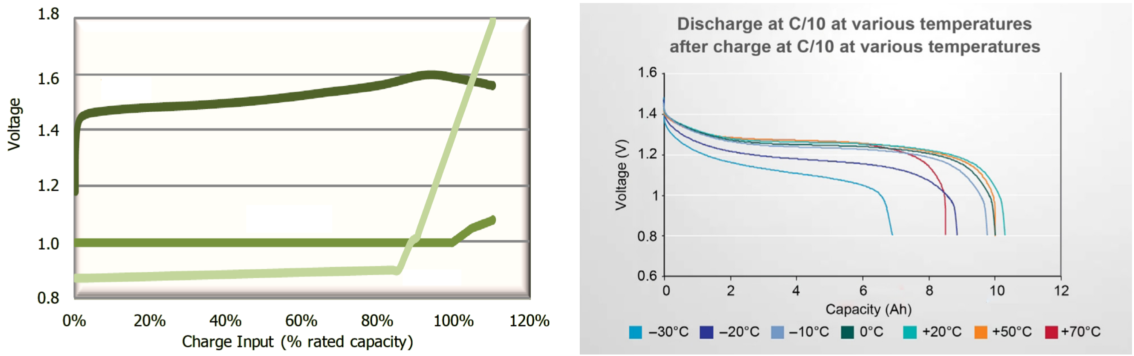

(a) A charge curve for a NiMH battery. The voltage initially spikes, then gradually increases with a bump towards the end. Note the sudden increase in battery temperature, as charging the battery is an exothermic process [22].

(b) Discharge curves for a NiMH battery at a range of different temperatures. Significant loss of capacity only occurs at extreme temperatures, making the battery highly suitable for operation under more severe weather conditions [23].

Figure 6: Typical charge and discharge curves for a NiMH battery.

Nickel metal-hydride cells have a typical OCV of 1.3 V. This is quite similar to the sea-salt battery, which when charging had a voltage of around 1.8 V, and a discharging peak voltage of around 1.7 V. Their specific energy is approaching lithium-ion batteries (currently 80 - 100 Wh/kg vs 100 - 265 Wh/kg), with higher maximum specific power (up to 1000 W/kg) [23]. Depending on the depth of charge and discharge, the energy efficiency can lie anywhere between 60% and 95%. High-end commercial NiMH battery systems can see lifespan of 10 - 20 years. Per example, the 2001 version of the Toyota Prius contains a NiMH battery, and it was found to have negligible to no degradation at all after 10 years [24]. They can operate under a wide range of temperatures and conditions, which, combined with the high specific power, make them highly suitable as spinning reserves and high-demand off-grid applications. Figure 6 shows typical charge and discharge curves of a NiMH battery.

2.2 Sea Salt Batteries

Aqueous electrolyte based batteries have been a subject of study for several decades. Hasvold et al. describe a non-rechargeable seawater based battery that utilizes metallic magnesium as a sacrificial anode to power subsea control systems [25]. A similar design was proposed by Shen et al., replacing the magnesium with aluminium [26]. Both designs also rely on the available oxygen in the water, which severely limits the current density, and are corrosion-based, meant to be used in the open ocean.

There exist various publications that use unmodified seawater as an electrolyte as well, in combination with various different kinds of electrodes. Kim et al. pioneered a design for a dual-electrolyte flow battery, utilizing seawater at the cathode side with carbon paper as electron collector [27]. The anode side was composed of metallic sodium with an organic electrolyte, and a NASICON type material to separate the two sides. This resulted in a discharge voltage of 2.9 V (see Figure 7a), with a 73% average voltage efficiency, and 84% Coulombic efficiency. Importantly, the initial cycle did see an evolution of Cl_2, judging from the measured decrease in Cl^- in the seawater electrolyte. Senthilkumar et al. used a similar platform, replacing the carbon paper cathode with NiHCF [28]. This resulted in an increase of the discharge voltage at 3.46 V at 10 mA g^{-1}, retaining over 60% of the initial capacity after 200 cycles (see Figure 7b). They also evaluated replacing the Na-metal anode with hard carbon, resulting in a consistent Coulombic efficiency of 91% after 50 cycles, with an energy density similar to lead-acid batteries. Zhang et al. used the same platform and Na-metal as anode, but replacing plain carbon felt cathode with a carbon sponge [29]. This caused a significant reduction of the voltage gap compared to the original system by Kim et al., from 1.15 V to 0.46 V, with both an increase in discharge voltage and decrease in charge voltage.

Han et al. also delved into dual-electrolyte seawater flow batteries, designing a coin-type cell casing, and evaluating its performance under different flow conditions, current densities, and cathode and anode properties [30]. Preheating the carbon felt cathode decreased the voltage gap significantly between charging and discharging, as did enabling proper flow of seawater over the cathode. Both the charge and discharge voltage also reached stable values faster with the flow enabled (1 hr vs +5 hrs). Finally, it was found that adding an electrocatalyst to the cathode decreased the voltage difference even further, down to 0.45 V. Lim et al. published a similar type of battery, using a sulfonated polystyrene based electrode, capable of absorbing Na^+ into its lattice, to decrease the formation of a solid phase barrier around the electrode. Finally, Park et al. explored a version of the seawater flow battery, using carbon-based materials for both the cathode and anode side, and comparing the performance between a simple carbon felt (CF) and activated carbon cloth (ACC) with a high surface area [31]. Their results showed that the ACC showed an increase performance, expressed in a smaller voltage gap with lower nominal charge voltage and higher nominal discharge voltage, as well better energy efficiency (86% vs 71%) and higher power density (16.2 mW/cm^2 vs 5.5 mW/cm^2).

Seawater has also been proposed as electrolyte in non-Na type batteries. Wei et al. proposed using seawater in vanadium flow batteries, replacing deionized water to increase the solvability of $VOSO_4$. Doing so increased the solubility of V^{3+} but decreased mobility slightly, leading to a small increase in Coulombic efficiency while sacrificing energy efficiency (see Figures 7c and 7d) [32]. Yu et al. used seawater as an electrolyte for zinc-air batteries [33]. This lead to similar results to the vanadium flow battery; the system saw a slightly decreased maximum capacity and discharge voltage, depending on the current densities applied.

Considering the charge and discharge behaviour of the different types batteries seen in literature, it is clear that the behaviour when charging of the seasalt battery seen by Homan in his studies resembles the later sections of the different versions of the flow batteries more than lead-acid, lithium-ion or nickel-based batteries. While the flow batteries see an initial rise of voltage, both Homan's battery and the flow batteries subsequently only experience a steady-state level, even if these differ (3.8 V for the flow batteries vs 1.8 V for Homan's measurements). The discharge phase, however, seems to resemble the discharge phases of the more typical commercial batteries more, with the slow voltage decrease during most of the discharge phase, and a sharper drop towards lower SoC values, similar to the designs by two flow batteries by Senthilkumar et al. [28] and Park et al. [31], as well as the Vanadium flow battery and the Nickel-air battery by Wei et al. [32] and Yu et al. [33] respectively.

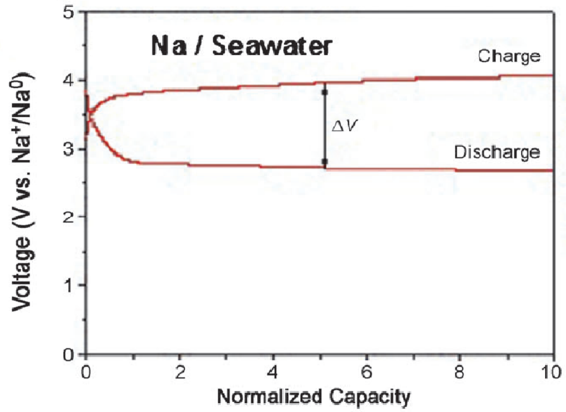

(a) charge-discharge curves for a dual-electrolyte seawater flow battery design [27].

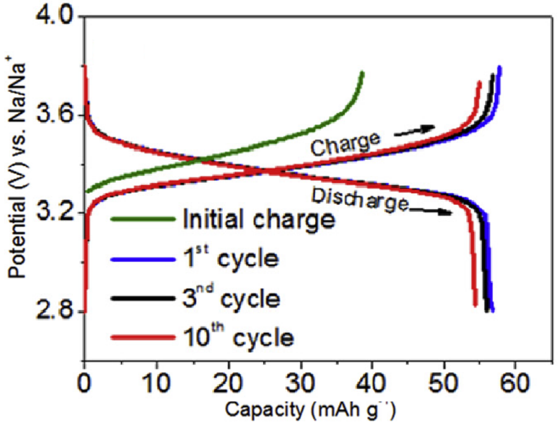

(b) Cycled charge-discharge curves using a swappable NiHCF cathode [28].

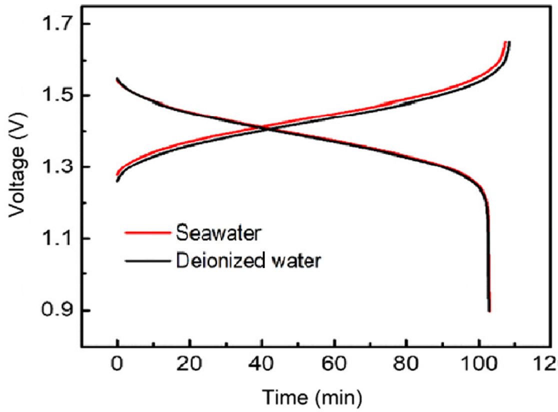

(c) Charge & discharge curves of the vanadium flow battery at 50 mA/cm^2 [32].

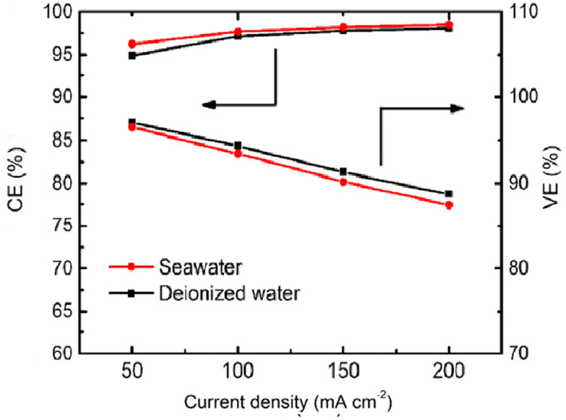

(d) Coulombic and voltage efficiencies of the vanadium flow battery at different current densities [32].

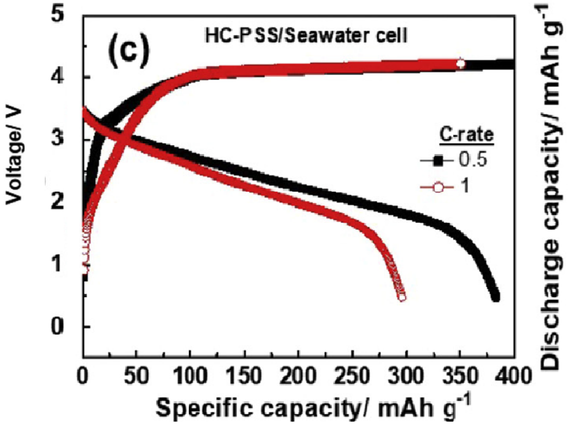

(e) Initial charge & discharge cycle for the HC-PSS sea-water battery [34].

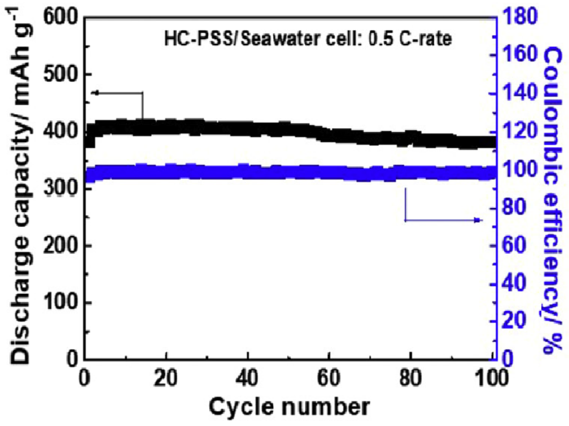

(f) Long-term coulombic efficiency and discharge capacity of th HC-PSS sea-water battery[34].

type	Areas of study	results	Year	Reference
Corrosion	In-situ operation	Explores Pt/C and Pt/WO_3 cathodes, H_2O reduction at 0.5 V, 5 mA/cm^2 with Ca/Mg$(OH)_2$ buildup, O_2 reduction at 1.4 V, 0.1 mA/cm^2. Consistent output over 21 days	1994	[26]
Corrosion	In-situ operation	650 kWh battery, 28 W, 1.4 W self-discharge	1997	[25]
Dual-electrolyte	One-step cathode synthesis with improved performance	Coulombic efficiency 84.5% vs 57.7% normal, 1500 cycles at 10 A/g in seawater	2022	[35]
V-redox flow	Use seawater vs deionized water for V-flow battery electrolyte	Replacing deionized water with seawater increases V-complex solubility (12% increase) to almost no detriment of performance	2019	[32]
Dual-electrolyte flow	Design proposal, operational performance	NiHCF cathode, 3.4V discharge, 80% capacity retention after 100 cycles, 60% after 200 cycles. 146 Wh kg-1, 10 mA/g	2017	[28]
Dual-electrolyte flow	Build casing for battery design, measure influence of flow rates, electrocatalysts	NASICON works, high flow rate decreases dV, 3.0 V discharge, electrocatalysts matter but finding a cheap one is hard	2018	[30]
Dual-electrolyte flow	Improve performance through cathode design	activated carbon cloth increases surface area, hence current density, dV, and other metrics. (dV 0.49 V, 86% eff$_E$, 16.2 mW/cm^2 vs 1.24 V, 71%, 5.5 mW/cm^2	2020	[31]
supercapacitor	Producing sustainable cathode from organic waste	130 F/g, 7.74 Wh/kg, 98% at 10,000 cycles	2021	[36]
Dual-electrolyte flow	General design and overall operation	HC-PSS overperforms vs other reported electrodes at all currents (383 mAh/g at 0.5C, 295 mAh/g at 1C), high discharge capacity at 1C without capacity loss, consistent discharge capacity after 100 cycles, 99.5% Coulombic efficiency, Sb-C materials have low capacity (372 mAh/g at 50 mA/g)	2021	[34]
Dual-electrolyte flow (Zn)	Replacing deionized water w/ seawater	very little to no difference to deionized water in potential and Pmax (136 mW/cm^2), slightly decreased capacity (724 mAh/g$_{Zn}$), 1.21, 1.18, 1.10, 1.00 discharge V at 5, 10, 25, 50 mA/cm^2	2020	[33]
Dual-electrolyte flow	General design and overall operation	2.9 V while discharging, Cl_2 evolution during first cycle, 73% voltage efficiency, 84% efficiency after 40 cycles	2014	[27]

2.3 DiBu-Model

There are many different ways to model a battery's performance, based on the purpose of the model; whether to represent the chemical processes in the battery itself, get an electrical representation of the battery to be incorporated in a high-resolution electrical system, or provide simple inputs for a general socio-economic model. Considering that modelling the battery is not the main focus of this work, the decision was made to model the battery with the model that was developed by Homan [13], named the Diffusion Buffer model (DiBu-model). The model was developed with implementation in energy management systems in mind, attempting to balance simplicity and accuracy. It derives its name from how heat storage devices operate under load.

Both types of storage experience the rate capacity effect, in which the the indicated capacity deviates from the actual capacity, depending on the rate of discharge. For heat storage devices, low rates of discharge causes reduced mixing of the water in the tank, leading to a temperature gradient. In batteries, high rates of discharge causes the electrodes to accumulate inactive species, 'artificially' decreasing the voltage, while plenty of active species may still be present (see Figure 9 for a a visual representation).

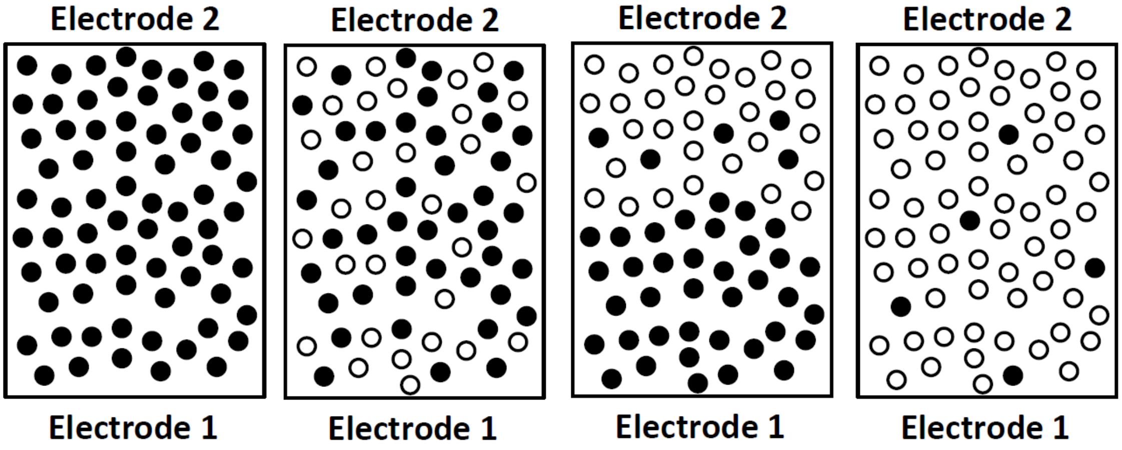

(a) (b) (c) (d)

Figure 9: A representation of the active species inside a battery (black) and the inactive counterparts (white) [13]. (a) Depiction of a fully charged battery. (b) Low discharge rates allow the battery to equalise while discharging. (c) At high discharge rates, electrode 2 makes it seem as though the battery is depleted, despite only being discharged for 50%. (d) Actual depletion of the battery.

The metrics that determine the processes are also similar. Both use a measure for available capacity (L vs Ah), available energy (L °C vs Wh) and flow (L/s vs A). The observed discharge behaviour is also similar, with the voltage or temperature remaining mostly level until sharply dropping when the storage medium is nearly fully discharged (see Figure 10) [13].

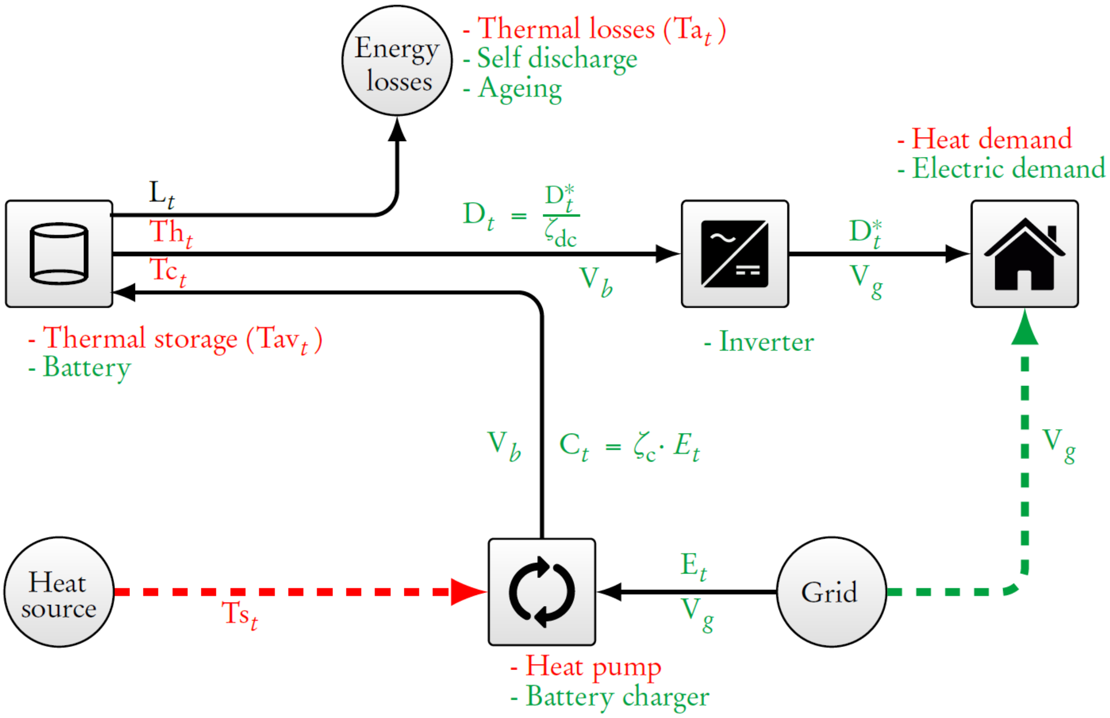

Figure 8: A schematic representation, showing the similarities between thermal systems and electrical systems. The thermal system is depicted in red, the electrical connection in green. Common connections are shown in black [13].

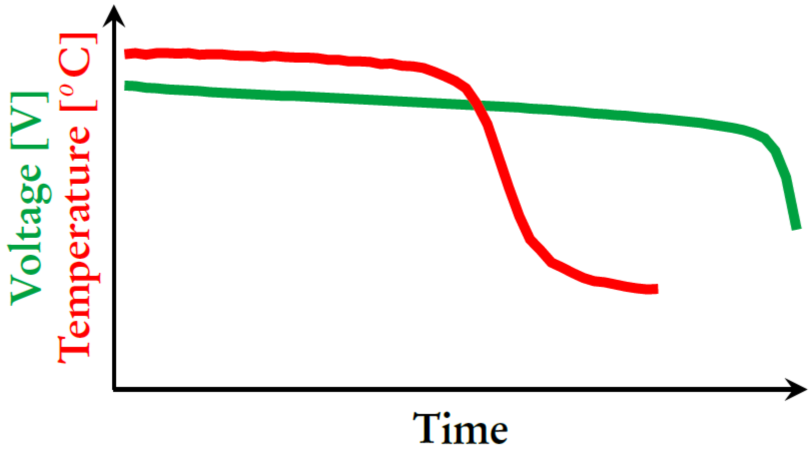

Figure 10: A comparison between discharge curves for a heat storage device and a generic battery [13]. The behaviour is nearly identical. Note that the temperature of the heat storage device cannot decrease beyond the ambient temperature while the voltage of the battery could technically decrease to 0 V if not for the safety limits.

The equations that make up the model can be found in Section 3.5.1.

2.4 Maximum Power Point Analogy To Voltage Time

Analysing the data pulled from the data sets and the measurements that were performed in-house, inspiration was pulled from photovoltaic cells to calculate a new metric.

In photovoltaics, the main metric that is used to determine the effective power is called the Maximum Power Point. The blue line in figure 11a represents the IV curve, plotting the current response to the applied voltage under standard conditions. The red line represent the resulting power, multiplying the applied voltage with the resulting current. The MPP is labeled, as the peak in the power curve corresponds to the ideal voltage and current to operate the photovoltaic cell at.

Since the data from both the measurements and the data sets resembles the IV curve of a photovoltaic cell somewhat, a new metric was introduced to characterise the curve in the charge and discharge curve, named the Maximum Voltage Time Point, after the MPP. While this metric holds no real meaning in terms of power supplied or State of Charge, it does provide a computationally efficient way to quantify the behaviour of the voltage curve around that point in both the charge and discharge phase. Figures 11b and 11c show how MVTP would work to quantify the point at which the transient phase transitions into steady state behaviour.

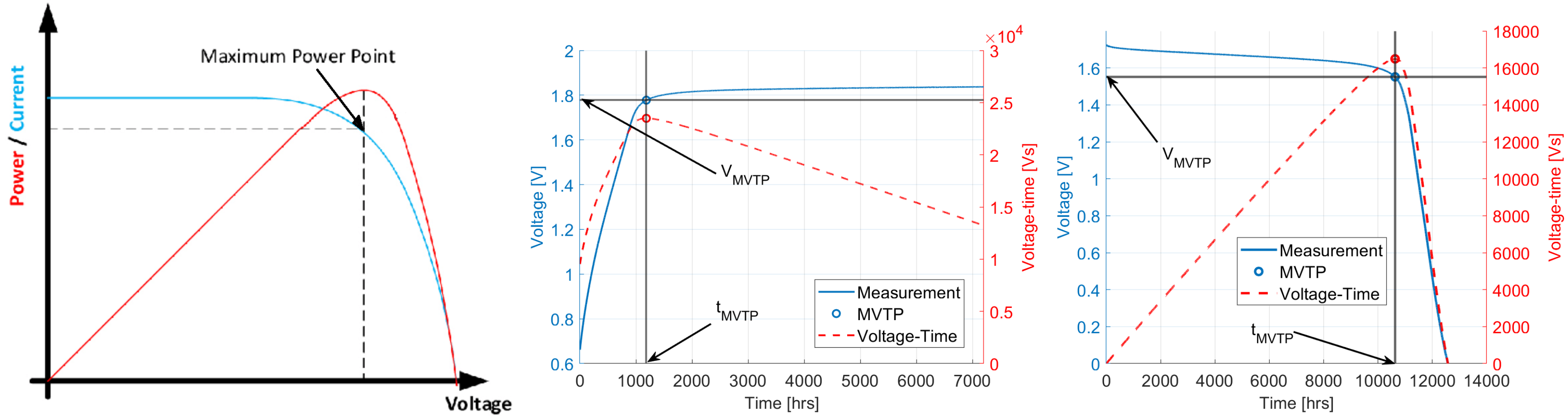

(a) A visual guide to the maximum power point (MPP) [37].

(b) The MVTP curve when charging. Data from in-house measurements.

(c) The MVTP curve when discharging. Data from in-house measurements.

Figure 11: A comparison between the IV curve of a photovoltaic cell and the charge/discharge curves of the sea-salt battery. The similarities in shape invited the creation of the MVTP, analogous to the MPP.

3 Methodology

This chapter will detail the analysis methods, battery cycling protocols, and equipment used to perform the cycling tests. Section 3.1 will briefly mention the platform used for data analysis. Section 3.2 lists all the equipment that was used to perform the measurements. Section 3.3 explains the protocols that were used to cycle the battery and cells in different ways. Finally, Section 3.5 will detail the equations that make up the DiBu-model.

3.1 Data Analysis

All data was analysed in MatLab, version 2019b. While the software used to control the hardware that cycles the batteries does give information on charge capacity, energy capacity, and other metrics, the decision was made to calculate these quantities in MatLab instead, to keep it consistent with the provided data sets.

3.2 Equipment & Materials

The measured battery was provided by Dr. Ten. It consists of 4 battery cells, connected in parallel with threaded graphite rods, capped with graphite nuts. The main body of the battery was taped together using wide transparent tape. A ring-style wire-end connector was added on each electrode to provide a connection point.

The battery was controlled using an Arbin LBT 22043. The battery was placed in a cardboard container, inside a temperature chamber. The temperature controls were connected to an Arbin Temperature Chamber Interface for precise control, but were ultimately deemed unnecessary due to stable conditions inside the lab. The battery was connected using crocodile clamps, with the measurement clamps placed onto the crocodile clamps. Images of the set-up can be seen in figure 12.

3.3 Battery Cycling

The battery was cycled multiple times, at constant current, and at constant voltage. Section 3.3.1 details the constant current protocols, while Section 3.3.2 details the constant voltage protocol.

3.3.1 Constant Current

To test the battery, a specific charge-discharge cycle was recommended by Dr. Ten. This involved a simple two-step process. First the battery was to be charged at 200 mA, for 7 hours, for a total of 1.4 Ah charged. Then, the battery was to be discharged at 200 mA, until the voltage of the battery reached 0 V. All subsequent constant current measurements were based on this principle idea; charging with a time limit, followed by discharging with a voltage limit.

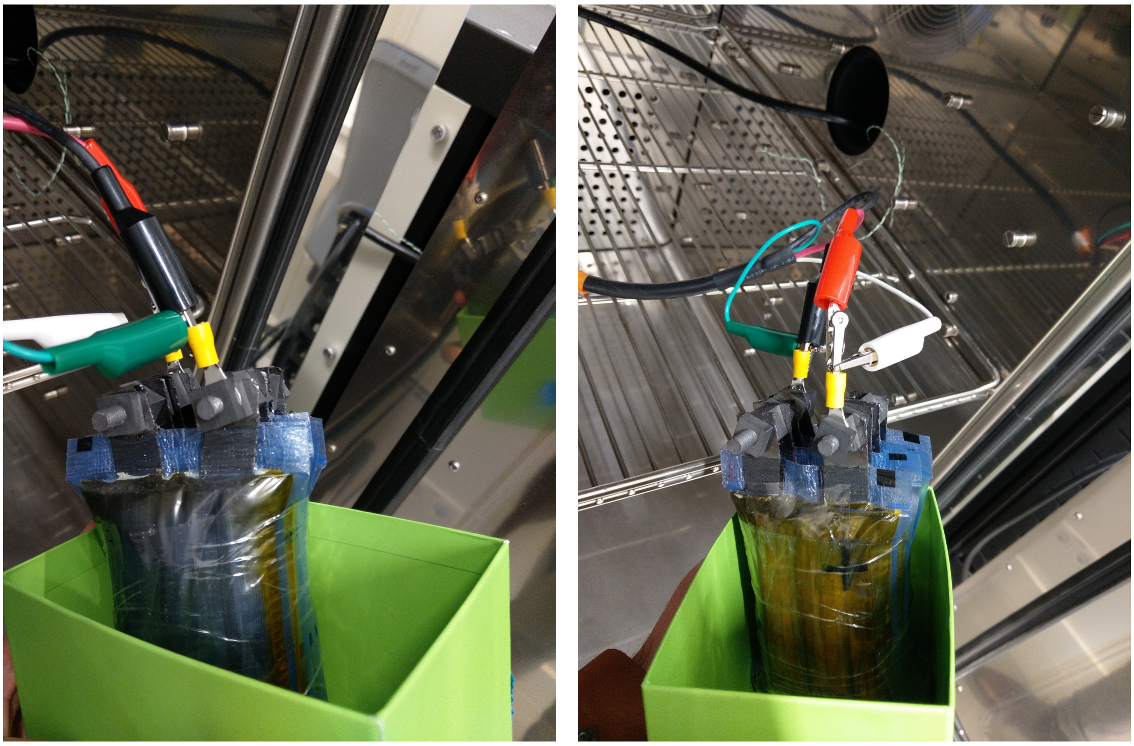

(a) One angle of the setup. (b) Another angle of the setup.

Figure 12: Two photos depicting the setup used to cycle the battery. The container was placed inside the steel chamber prior to activating any cycling protocols.

All constant current measurements were programmed to charge the battery for a specific time duration, and discharge the battery until 0 V was measured. An equal and opposite current was applied for charging and discharging. Figure 13 shows a flow chart showing the individual steps. A rest period was added in front of the charging step to be able to record the voltage of the battery before charging. Table 2 shows an overview of the total charge duration for each measurement at each applied current.

The battery measurements were performed at 50 mA, 100 mA, 150 ma, 200 mA, 250 mA, and 300 mA. A total approximate amount of 1.4 Ah, 1.12 Ah, 0.93 Ah, and 0.8 Ah was charged at each current level. When programming the charge phases, a time cut-off was used. Table 2 shows the total charge time for each current level and total amount of charge.

The battery was then subjected to a repeated set of measurements at 200 mA, following the corresponding values in the table. Then the battery was cycled 8 times at 200 mA following the constant-current flow chart, charging for 4 hours. Finally, a last set of measurements was done at 200 mA, in reverse order from the table (labeled 'Reverse').

The battery was also cycled between 1.45 V and 1.85 V a total of 10 times. Figure 13c shows the corresponding flow chart. The results can be seen in Section

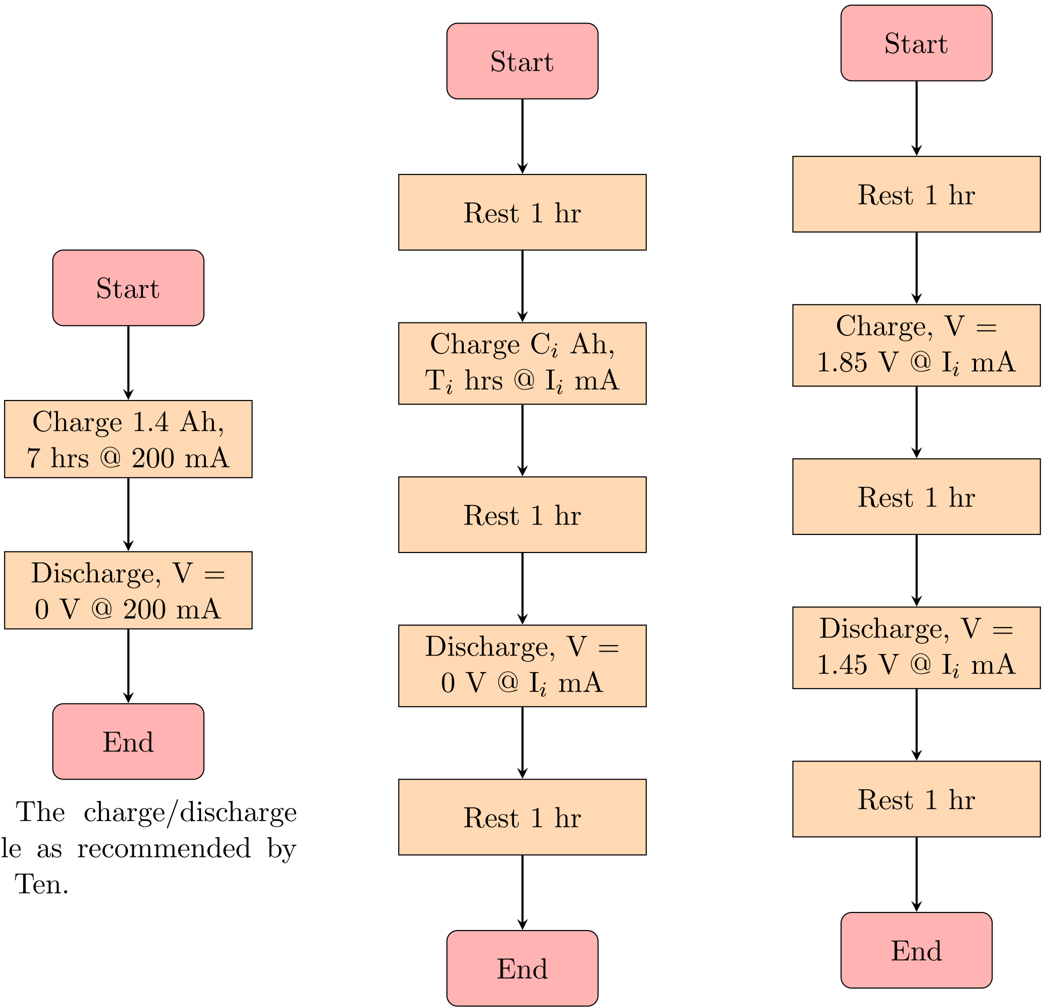

(a) The charge/discharge cycle as recommended by Dr. Ten.

(b) The generic constant current charge/discharge cycle.

(c) The charge/discharge cycle used for the voltage-limited constant current charge/discharge cycle.

Figure 13: Flow charts for the constant-current measurements. The initial rest period was introduced to record the voltage of the battery prior to charging. The generic cycle used for all measurements after the initial set at 200 mA. In the actual programming of the charge phase, a specific amount of time was set, but since these measurements are done at constant current, time and total charge are interchangeable.

Table 2: The total charge time in hours for each charge step, for each applied current level and approximate total charge.

		Total charge [Ah]			
		0.8	0.93	1.12	1.4
Current [mA]	50	16	18	22	28
	100	8	9	11	14
	150	5	6	7	9
	200	4	4.67	5.6	7
	250	3.2	3.75	4.5	5.6
	300	2.6	3.1	3.75	4.6

5.5

4 Individual cells were cycled for a total of 20 times, using the same generic constant current cycle described in figure 13b. The electrodes were connected in a similar fashion to the battery, with the aligator clamps directly clamped onto the carbon paper-based electrodes of the cells.

3.3.2 Constant Voltage

To find the maximum capacity of the battery, a set of measurements was conducted at constant voltage. The battery was first left to rest for 10 minutes. The intent was to charge the battery at 1.8 V until the current value reached 0 A. However, considering the data, the decision was made to cut the charge phase when the change in current approached 0 A/s. Due to software limitations, this had to be done manually. The battery was then left to rest one hour. It was then discharged at a fixed 150 mA, until the voltage measured 0 V. Finally, the battery was left to rest for one hour. This cycle was repeated three times in total. Figure 14 shows the protocol in flow chart form.

3.4 MVTP Calculations

The process to calculate the MVTP values differs slightly between the charge and discharge phase. For the discharge phase, the time values were multiplied with the corresponding voltage values. Then the maximum value was found using matlab function *max*. This value was used to find the index number for the corresponding time and voltage. For the charge phase, the exact same steps were followed, save for one exception. Before the multiplication of the time and voltage values, the time axis was first reversed, i.e., the first voltage measurement was multiplied with the last time value.

3.5 Modelling

The data from measuring the battery at 200 mA was fitted to the DiBu, as developed by Homan [13]. The equations that make up the model, and the steps to define its constants, are detailed below.

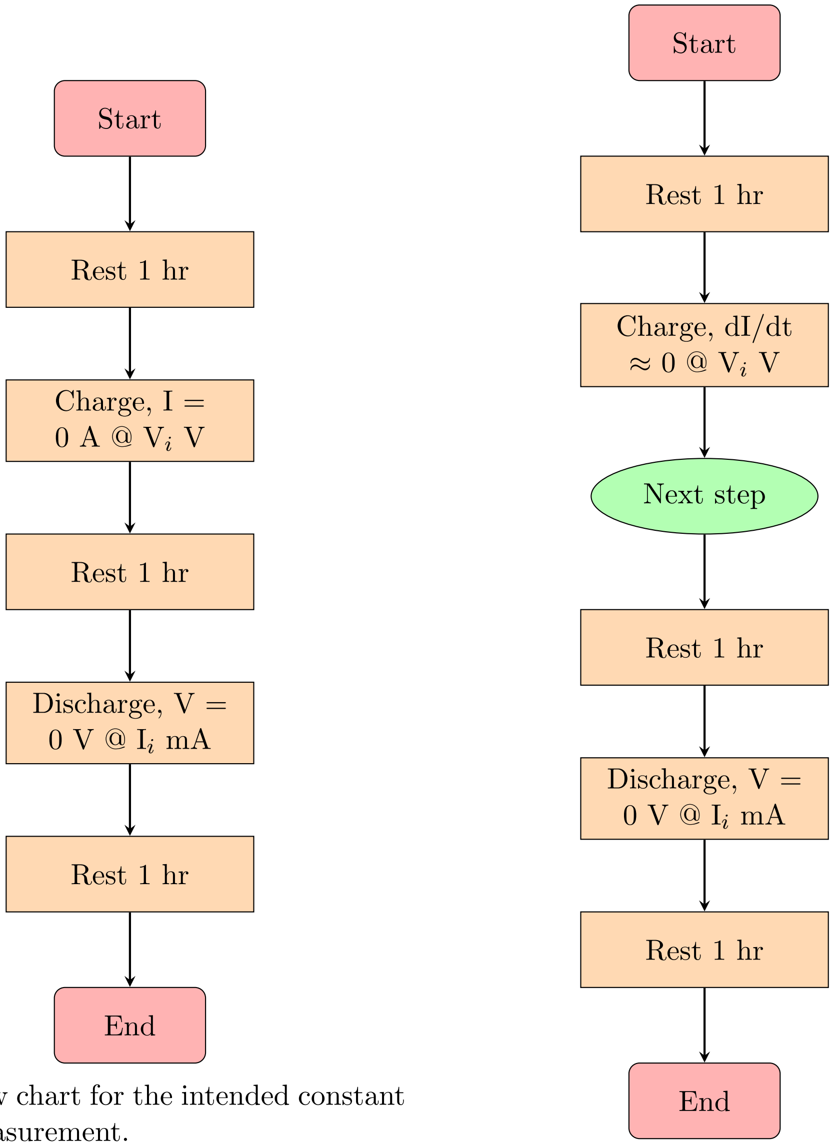

(a) The flow chart for the intended constant voltage measurement.

(b) The constant voltage measurement as executed in practice.

Figure 14: flow charts depicting the constant-voltage measurements. Note the change in rest period before charging, and the altered end condition for the charge phase.

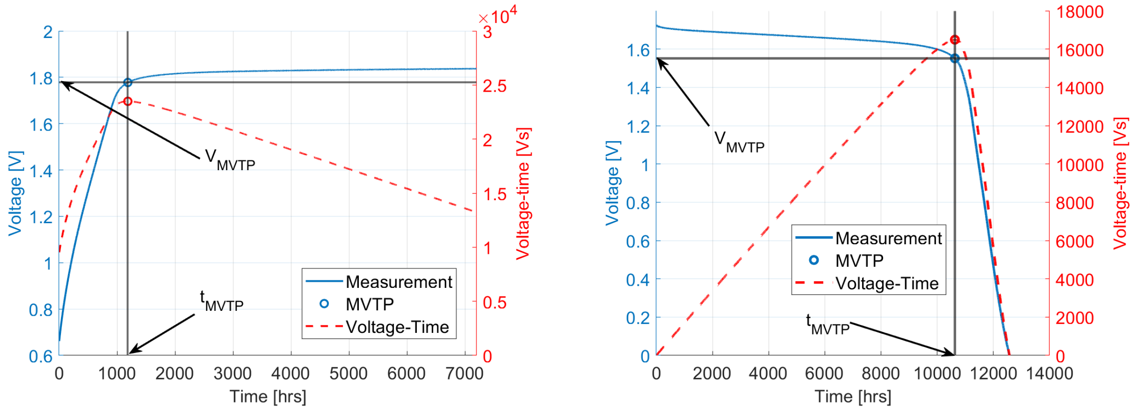

(a) MVTP visualised for the charging cycle.

(b) MVTP visualised for the discharge cycle.

Figure 15: Visualisation for the MVTP concept for charging and discharging.

3.5.1 DiBu-Model

The DiBu-model consists of a set of 7 equations. It separates the operation of the battery into four different phases; charging, post-charge rest, discharging, and post-discharge rest. Considering time interval [t',t], and E_{max} as the total energy capacity of the storage device, the time-dependent SoC can be defined as

$$SoC_t = SoC_{t'} + \frac{\Delta E_{t',t}}{E_{\text{max}}}, \tag{1}$$

with

$$\Delta E_{t',t} = \overline{U} \cdot \overline{I} \cdot (t - t'). \tag{2}$$

with average battery voltage $\overline{U}$ and applied current $\overline{I}$ during time interval [t',t]. Assuming constant $\overline{I}$, several equations are defined for each phase in the battery operation to define the change in voltage in time interval $[t_{j-1}, t_j.]$

While discharging the battery over time interval $[t_{j-1}, t_j.]$, the model describes the voltage behaviour as

$$U_{t_j} = U_{t_{j-1}} + \frac{\alpha \cdot \overline{I} \cdot (t_j - t_{j-1})}{SoC_{t_{j-1}}}. \tag{3}$$

When the battery is charging, this model assumes there is a voltage increase that is strictly linear, following

$$U_{t_j} = U_{t_{j-1}} + \frac{\overline{I}}{\delta}. \tag{4}$$

However, this assumes a constant time-step while measuring and/or predicting the next step. To allow for variable time-steps, an adjustment was made, leading to the equation

$$U_{t_j} = U_{t_{j-1}} + \frac{\overline{I}}{\delta} \cdot (t_j - t_{j-1}). \tag{5}$$

An alternative is suggested by Homan based on his findings, where the voltage remains constant throughout the charging phase, with an offset that scales with the amount of current. This leads to the equation:

$$U_{t_j} = U_{\mathrm{OCV}} + \sigma \cdot \overline{I}. \tag{6}$$

If left at rest after charging, the voltage remains unchanged, which the model describes as

$$U_{t_j} = U_{t_{j-1}}. \tag{7}$$

Finally, the DiBu-model uses an first order system approximation for the voltage during the rest phase after discharging, following equation

$$U_t = U_{t'_0} + (U_{\max} - U_{t'_0}) \cdot (1 - e^{\frac{t-t'_0}{\tau}}), \tag{8}$$

with U_t the voltage of the battery at time t, and $U_{t'_0}$ the voltage of the battery at the start of the rest phase after discharging. U_{max} is defined as the highest battery voltage in the preceding discharge phase. An attempt was made by Homan to define τ as a constant [13], but it was found to be a function of time as well.

$$\tau = \beta \cdot (t - t'_0) + \gamma. \tag{9}$$

α, β, γ, δ and σ are all presumed to be battery dependent constants.

Matlab was used to identify the model constants for each data set. For the rest phase after discharging, the built in function *lsqnonlin* was used to curve-fit the objective function. For the discharge function, a different approached was used, due to the recursive nature of the equations. A loop was created to evaluate a wide range of values. Then the total sum of error was calculated between the large set of predictions and the measurements. The value corresponding to the lowest total sum of errors was then used to repeat the process with a more narrow range of possible inputs, while increasing the amount of significant numbers.

4 Dr. Ten Data Set Analysis

In this Chapter, all the results from the data analysis of the data sets provided by Dr. Ten will be presented. Section 4.1 details the general trends and patterns found in the data sets. Section 4.1.1 briefly touches on the voltage behaviour in rest. Section 4.1.2 sees the application of the concept of MVTP. Finally, Section 4.2 will detail some of the problems and potential pitfalls found in the data sets.

4.1 General trends

All combined, the three data sets encompass just under 1050 cycles, with the smallest set, BT1, containing only 26 cycles, BT3 49 cycles, and BT2 964 cycles. All the full cycles use the same amount of current for charging and discharging, i.e., if 200 mA was used to charge the battery, 200 mA was used to discharge the battery as well. The entirety of BT3 was measured at 200 mA charging and discharging, while BT1 sees a wider variety, with 200 mA and 300 mA measurements making up the vast majority of all cycles. BT2 was measured at a much lower current (50 mA), possibly due to the battery containing fewer cells than the batteries used in BT1 and BT3. BT1 was the only data set that used a variety of different currents, ranging from 100 mA up to 1,000 mA. The measurements at higher currents had a reduced total charge time.

Almost all charge phases in BT1 lasted exactly 1 hour, with a small set utilizing higher currents (>400 mA) lasting half an hour. The voltage follows a consistent pattern every time; there is an initial transient phase which sees a sharp increase in voltage, which starts to level off at around 1.6 V. Finally the voltage reaches steady state at around 1.8 V, correlating to the magnitude of the current. The voltage behaviour scales with current; higher currents correlate to steeper increases in the transient phase, as well as higher final voltages.

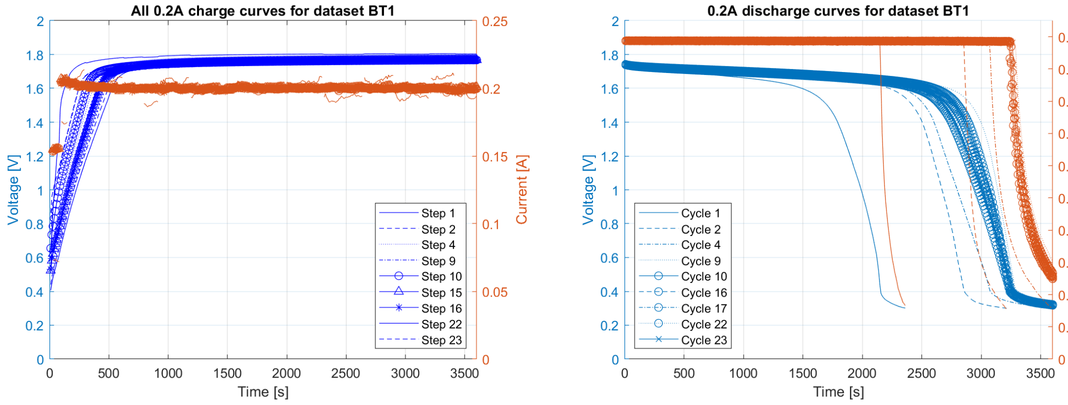

(a) Charge curves for all cycles with 0.2 A. The basic shape of the voltage curve is consistent between each cycle, except for cycle number 1 (left most solid blue line).

(b) Discharge curves for all 0.2 A discharge cycles. Note the decrease in current at lower voltage levels, and subsequent change in voltage change.

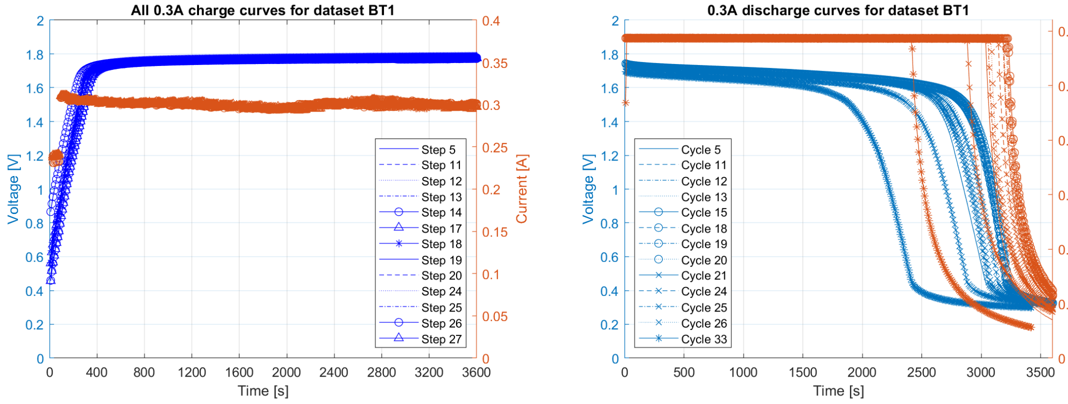

(c) Charge curves for all cycles with 0.3 A. As with the 0.2 A charge curves, the voltage curves show consistency throughout the experiment, with varying start voltages.

(d) Discharge curves for all 0.3 A discharge cycles. Note again the sudden decrease in current at lower voltage levels, as well as the slightly larger spread in starting voltage.

Figure 16: Charge and discharge curves at 200 mA and 300 mA.

The same pattern can be seen in reverse when discharging the battery; throughout most of the discharge step the voltage remains almost constant at around 1.7 V, then sees a transient phase as the voltage drops sharply from around 1.55 V. The long tail at the end of the measurements coincides with a sharp decrease of the current as the voltage falls below 0.4 V. Similar to the charge phase, the voltage characteristics correspond to the applied current, with higher currents leading to lower steady state voltages and sharper transient phases. Note that the voltage is not cut off at 0 V, contrary to Dr. Ten's recommendations for discharging the battery. However, it was communicated that the equipment used to generate these data sets was meant for testing NiCd batteries, which have a safety cut-off voltage of 0.3 V.

The charge phases are consistent. The rate at which the voltage climbs in the transient phase is unchanged between different cycles, and seems to taper off at the same voltage every time. The voltage of the measurements at 200 mA do seem to reach the constant voltage region at different moments in time, which correlate to the initial voltage. At 300 mA, this difference becomes even smaller, with the charge voltages nearly overlapping one another despite the deviations in starting voltage.

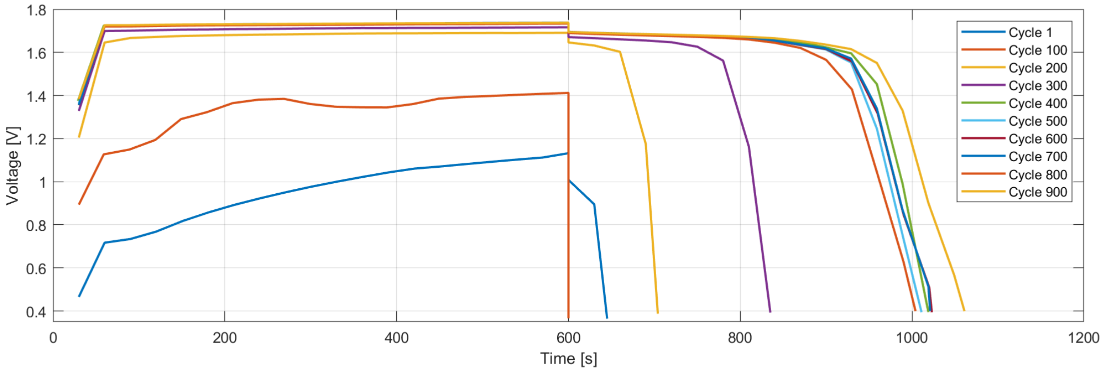

(a) A selection of charge/discharge cycles from the BT2 data set. Cycles 1, 100, 200 and 300 still show unique voltage patterns. After cycle 300, all other cycles are nigh identical in behaviour.

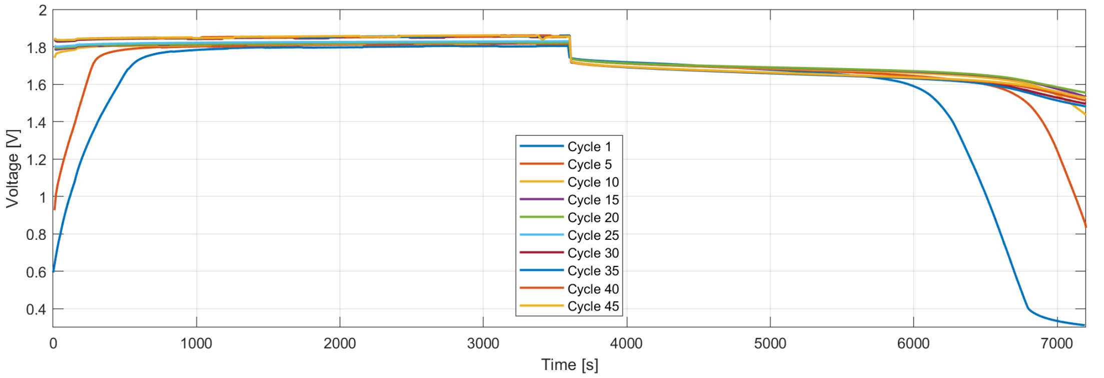

(b) A selection of charge/discharge cycles from the BT3 data set. Only cycle 1 and 5 are distinguishable. All other cycles are nigh identical, and show clear signs that the battery is not fully discharged during the discharge phase.

Figure 17: A selection of charge/discharge cycles from data sets BT2 and BT3.

The general patterns found in data set BT1 can also be found in data sets BT2 and BT3. In the case of BT2, all charge and discharge steps were performed at an average of 0.05 A, with the actual values varying between 0.04 A and 0.06 A. Each charge and discharge step lasted for 600 seconds, which measurements done every 30 seconds. As such the resolution of the measurements is quite low, as can be seen in figure 17a.

Although BT2 uses a different magnitude of current, it shows the same behaviour in voltage, possibly because of a decreased battery size (perhaps just a single cell), while the BT3 seems to use a similar sized battery. In all cases, the typical cycle starts with a sharp increase in voltage followed by a levelling off at around 1.8 V while charging, after which follows the same very slow decrease from 1.75 V to 1.6 V and its subsequent sharp drop towards the cut-off voltage during the discharge phase.

All data sets show remarkably high efficiencies. BT1 peaks at 95% Coulombic and 85% energy efficiency, BT2 seems to achieve near 100% Coulombic efficiency, and BT3 consistently pushes 97 % Coulombic efficiency and around 90% energy efficiency. These numbers are extraordinarily high, especially over repeated measurements like in BT2. Coupled with the consistent amount of energy discharged over time, the battery shows no sign of aging at all.

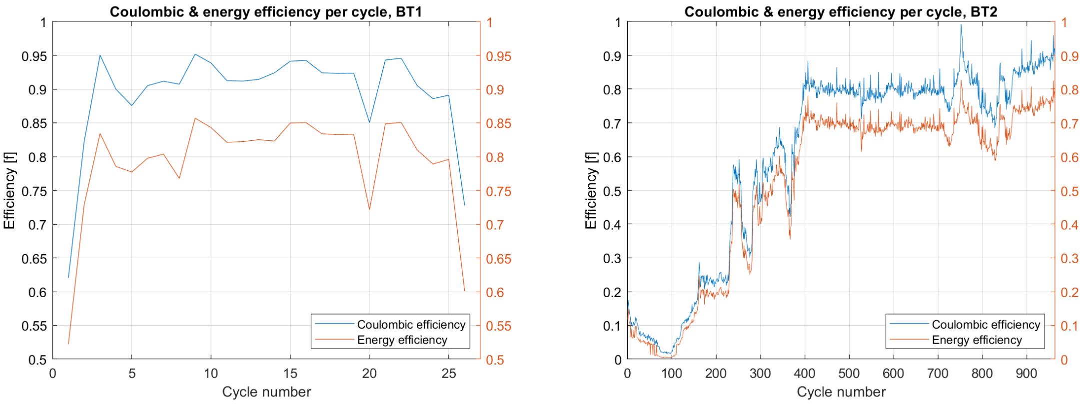

(a) The first and last cycles show the lowest efficiency.

(b) The first set of cycles show incredibly low efficiency, possibly due to the size of the battery itself.

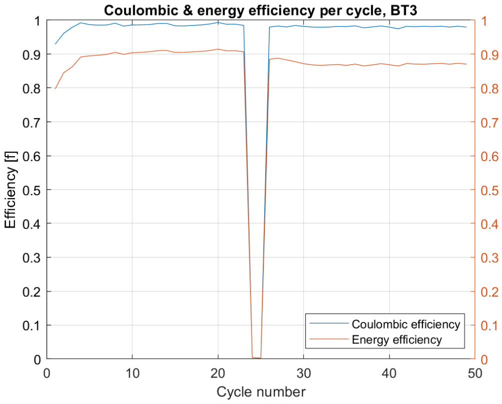

(c) The efficiency is consistent throughout the measurement.

Figure 18: Efficiencies per cycle for each data set.

The efficiency numbers for the first set of cycles of BT2 are low compared to the rest of the data set. The charge phases only see the end voltage slowly creep up, at around 0.1 V at a time, with the discharge phases being incredibly short. It is possible that the battery is grossly undersized for the amount of current pushed into it, causing the battery to be operated in an unstable region where charge retention is low. The fact that the final voltage at the end of each charge phase is a little higher than the previous charge phase, does mean that the discharge phase does not fully discharge the battery, leaving some charge for the next cycle to build on. Unfortunately, due to the low resolution of the data, most of the State of Charge region that sees large voltage changes is lost, so no further in-depth analysis can be made.

4.1.1 Voltage Decay & Recovery

BT1 features two Sections in which the battery is left to rest for a period of 6 hours, one after a charge cycle, one after a discharge cycle. After the discharge cycle the voltage increases strongly, from 0.45 V to 0.81 V. After the charge cycle, the voltage loss is quite small, from 1.775 V to 1.75 V. Figure 19 shows the relevant curves.

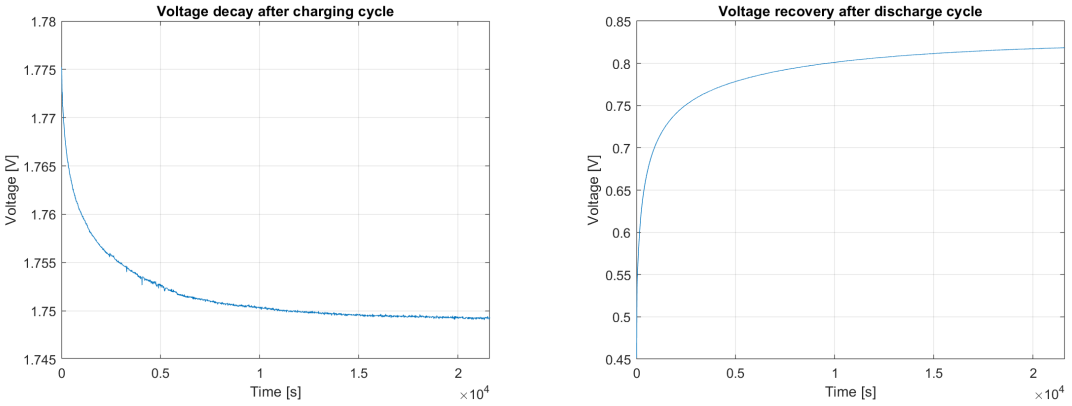

(a) The voltage decay after charging is quite small, less than 2%, and for all intents and purposes can be considered to be zero.

(b) There is a significant recovery in voltage post-discharging, which should be taken into account.

Figure 19: Graphs showing the voltage decay and recovery after a charge and discharge cycle respectively.

While the voltage loss after charging is minimal, the large change in voltage after discharging is an example of the rate capacity effect, and tells us that the rate of discharge is outpacing the rate at which internal diffusion mechanisms homogenize the electrolyte solution. The voltage does not seem to recover all the way back to near-OCV levels, meaning the difference is not extreme, but lower discharge currents should be evaluated to see if that increases the amount of usable capacity in a single discharge.

4.1.2 Voltage-Time

Using the concept of MVTP (as described in Section 2.4), approximate values were found to characterise the onset of the quasi-constant voltage region when charging, and the onset of the hard voltage decay when discharging. These results could only be found with any resolution for data set BT1, as the resolution of BT2 was too low, and the charging voltage curves for the later cycles of BT3 no longer show the same behaviour. Figure 20 shows the results for data set BT1, at 200 mA and 300 mA specifically.

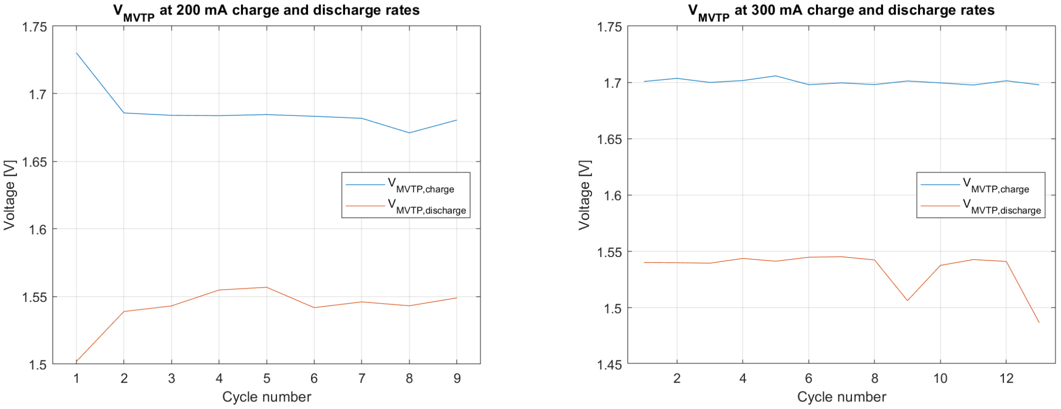

(a) Only the first measurement of the data set shows significant deviation at 200 mA. The other cycles show consistent values.

(b) V_{MVTP} is 1.7 V on average. The discharge phases show some more variability, with most reaching 1.55 V, and two outliers at lower values.

Figure 20

Apart from the very first measurement at 200 mA (also the first measurement in the data set), the results are remarkably consistent. At 200 mA, the MVPT voltage occurs around 1.67 V, with one slight dip at 1.65 V. Likewise, when discharging at 200 mA, it consistently hovers around 1.55 V, with some measurement just over and the other just under that voltage. At 300 mA, the values when charging are even more consistent, at 1.7 V for every charge phase. The discharge phases also show consistent results at just under 1.55 V, with two outliers at around 1.5 V.

4.2 Inconsistencies

Despite these findings, the three data sets do contain a number of problems. The resolution of the data for BT2 is rather poor, with only 20 measurement points per charge/discharge phase, compared to just over 370 measurements per phase in BT1. Because of this poor resolution, while general conclusions can be drawn, and some average efficiency can be calculated, further analysis, e.g. MVTP calculations, are impossible to perform reliably.

Data set BT3 has its own particular set of problems. All charge and discharge phases last the same amount of time (maximum of 3600 s), and all are performed at 200 mA. However, the data shows that there is a steady accumulation of charge inside the battery, as the terminal voltage at the end of each subsequent discharge phase increases, up to 1.4 V. This happens despite the fact that for the first 5 cycles, the data set reports that the battery reaches the cut-off levels while discharging. Considering the rate capacity effect, the applied current may be too high, leading to the measurement reaching the cut-off voltage before the concentrations of active species inside the battery had time to equalize. This begs the question in what ways the battery used for BT3 differs in construction and size to BT1.

The discharge phases in BT1 also show some inconsistencies. While the charge phases are nearly identical apart from the initial voltage and some deviations towards the end of the transient phase, the discharge phases show larger variations; especially at 300 mA, the initial voltage and the onset of the decline varies greatly between measurements. At 200 mA, there is a similar spread, although less pronounced. Considering that these measurements were performed back to back, one could question why these discharge phases do not show identical behaviour.

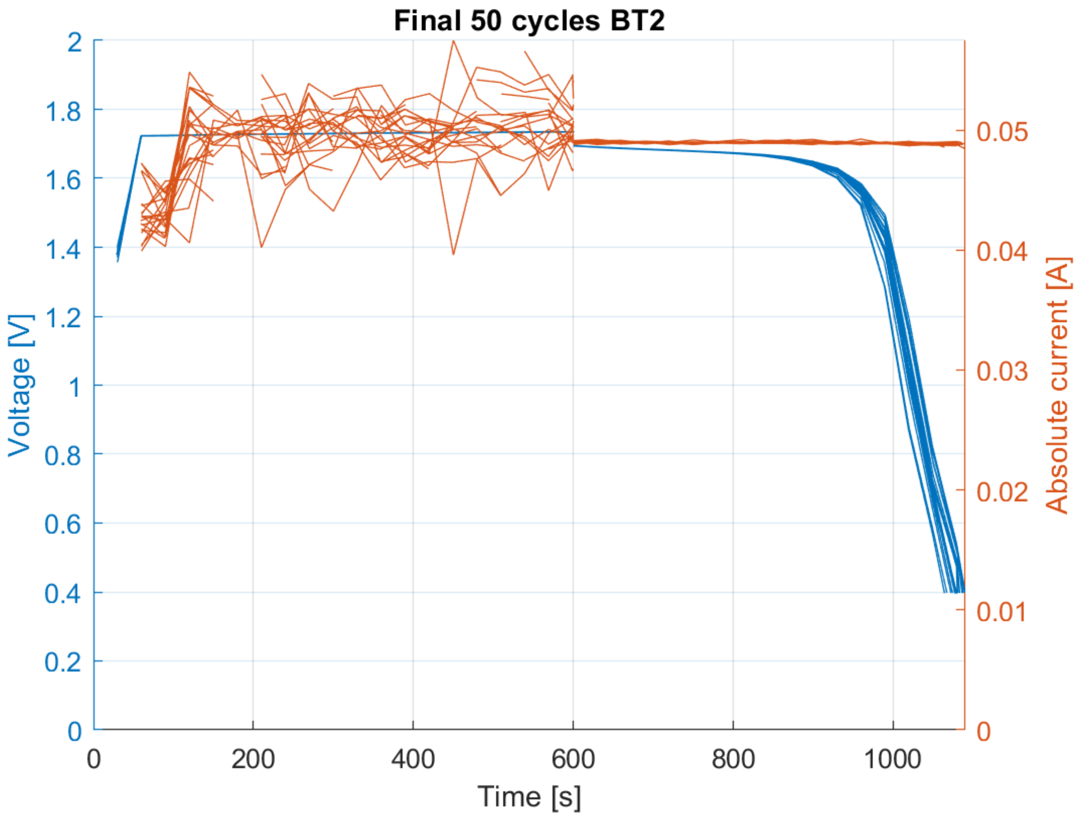

Figure 21: The last 50 cycles of BT2. The current during the charging phase is highly variable, while the discharging current is more consistent. Also note the lack of data points; the entire phase of rapid voltage increase is reduced to a single data point.

There also seems to be some form of equipment problem throughout the data set. Figure 21 shows the last 50 cycles of data set BT2. It clearly demonstrates the difference in current consistency between the charge phase and discharge phase.

While discharging the current stays at a consistent 50 mA. While charging however, the current jumps up and down, between 40 and 60 mA, with occasional outliers in both directions. This casts some doubt on the results of these measurements. This instability of the applied current while charging is also found in BT1 and in BT3. The measured voltages seem stable, but one should wonder to what extent the results have been influenced by possibly malfunctioning or unsuitable equipment. Furthermore, while the current is clearly set to maintain a consistent value, many datapoints are missing; in the charge phases measured in BT1, between 4% and 13% of the current measurements are missing, similar to BT3. Due to the low resolution, in BT2 the percentage fluctuates between 5% and 20%.

Furthermore, The charging voltage seems to become more reactive to the amount of current pushed through, even mid-measurement; while it is expected for a battery's voltage to scale with the amount of current forced into or out of it, in BT3 this effect becomes more pronounced as shown in figure 22a. However, the voltage is also starting to show ripples that are not related to current, with an increasing ripple starting to occur towards the end of the charging cycle. Figure 22b shows an example of this behaviour found in BT1. The resolution of data set BT2 was too low to properly observe this behaviour. What causes this effect is unknown.

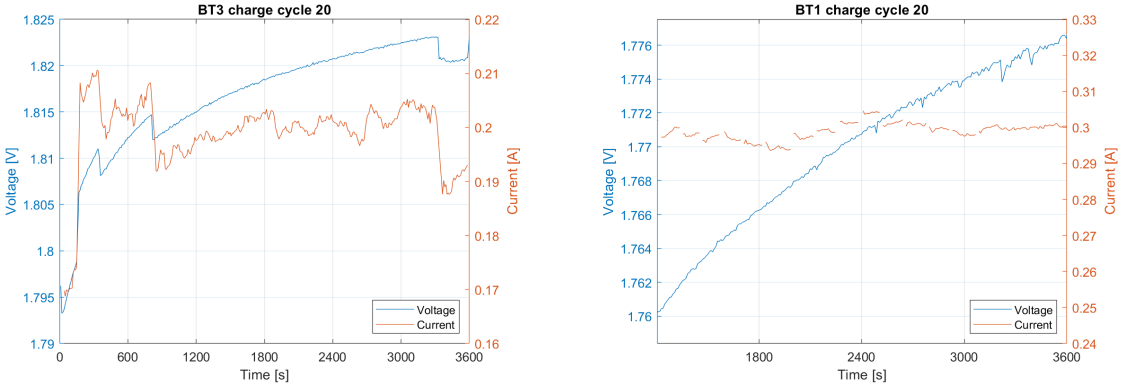

(a) Charge cycle 20 of BT3 shows how the voltage responds strongly to strong changes in current, as well as the low-level ripple throughout the charging cycle.

(b) Charge cycle 20 of BT1 shows an increasing ripple in voltage levels as the charge cycles approaches its cut-off time.

Figure 22: Graphs showing the increasing voltage ripple as the voltage approaches peak levels.

Finally, as Homan also showed, the battery does not show the final increase in voltage towards the end of the charge phase, a trait that Li-ion, lead-acid and NiMH batteries do have. this is important since it provides an easy way to estimate the capacity; you simply charge the battery until you see the second voltage spike, at which point one can safely assume the battery is charged up to, or close to, 100% SoC. Considering that so far, none of the seasalt battery data (neither Homan's work nor the data sets) show this behaviour, which leaves one of twho options. The first option is that the battery operates similarly to the flow batteries. However, if that is the case, one would wonder why the discharge curves do not match. The second option would be that the batteries have never been fully charged up to 100% SoC, which begs the question why one would make the decision to run such time-consumings measurements at e.g. 50% SoC, and avoid 100% SoC as much as possible.

5 In-House Measurement Results & Discussion

This chapter will describe all the findings from the in-house battery cycling tests. Section 5.1 will go over general finding from the constant-current measurements, including the voltage behaviour and how they differ between different applied currents. Section 5.2 briefly details the results for the MVTP calculations. Section 5.3 will discuss the findings on the battery's capacity and efficiency. Section 5.4 discusses the results of the constant voltage measurement, while Section 5.5 sees the battery cycled between two voltages. Section 5.6 contains the results from the single cell measurements, while Section 5.7 goes over some of the physical changes the battery has undergone while performing the measurements. Finally Section 5.8 will detail fitting the DiBu-model to the measurement data.

5.1 General Trends

Similar to the data provided by Dr. Ten and Homan's work, all charging and discharging curves show the same overall shape; the charge curves start with a sharp increase in voltage, which proceeds to level out between 1.7 V and 1.8 V. The discharge curves follow the same pattern in reverse, with the voltage remaining mostly constant, and a sharp decrease towards the end of the measurement. Figure 23 shows the second charge and discharge step of the experiment at each applied current.

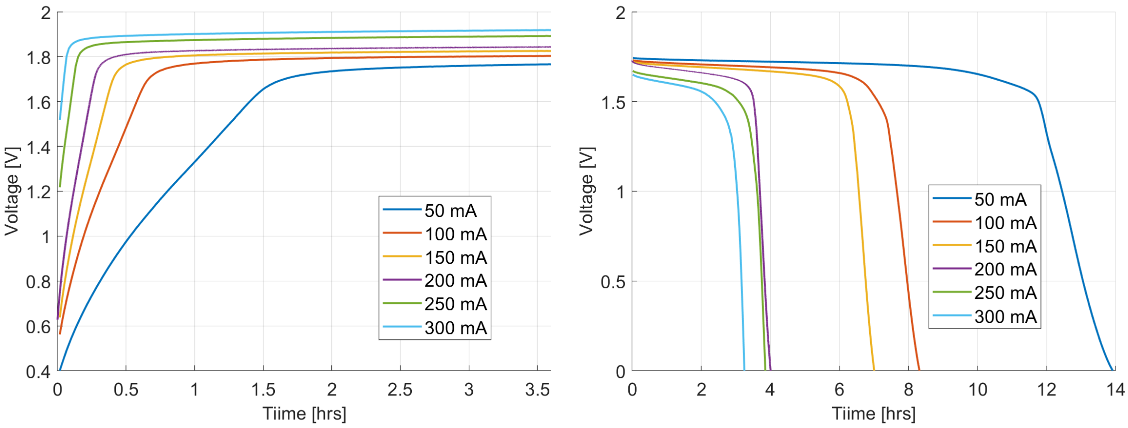

(a) Charging voltage curves at each applied current up until 3.6 hrs. The initial rate of voltage increase correlates to the amount of current used, as does the final voltage. Some measurements did take longer, but are not fully shown for the purpose of this graph.

(b) Discharging voltage curves at each applied current. The voltage drops at the end of the each measurement have almost identical slopes except for the 50 mA measurement. At higher applied currents (250, 300 mA), the initial near constant voltage region all but disappears.

Figure 23: Charge and discharge curves at every applied current. The voltage of the battery follows the same pattern as the data in the provided data sets.

While possibly trivial, it is encouraging to see little to no deviation in trends from the provided data sets to the in-house measurements. Similar voltage levels indicate that the internal chemistry is most likely the same, with similar I-V behaviour, despite using different equipment and possibly measuring the battery under different circumstances.

When charging the battery, the initial rate of voltage increase correlates loosely to the amount of current being pushed into the battery, as does the final voltage of the battery at the end of each measurement; the higher the current being pushed into the battery, the higher the battery's final voltage, with all terminal voltages lying between 1.75 and 1.9 V. Likewise, when discharging, the discharge time correlates to the applied current, with the 50 mA discharge step taking the longest time. The slope of the transient phase of the battery's voltage seems largely unaffected, with the 50 mA discharge step being the notable exception. At higher applied currents, the initial near-constant voltage phase seems to disappear; at 300 mA, the measured voltage drops noticeably from the start all the way to the end of the discharge phase. Inversely to the charging phase, when discharging, the highest applied currents show the lowest starting voltage; at 50 mA discharge current, the first voltage measurement shows 1.74 V, while at 300 mA, the measurement comes up at 1.65 V.

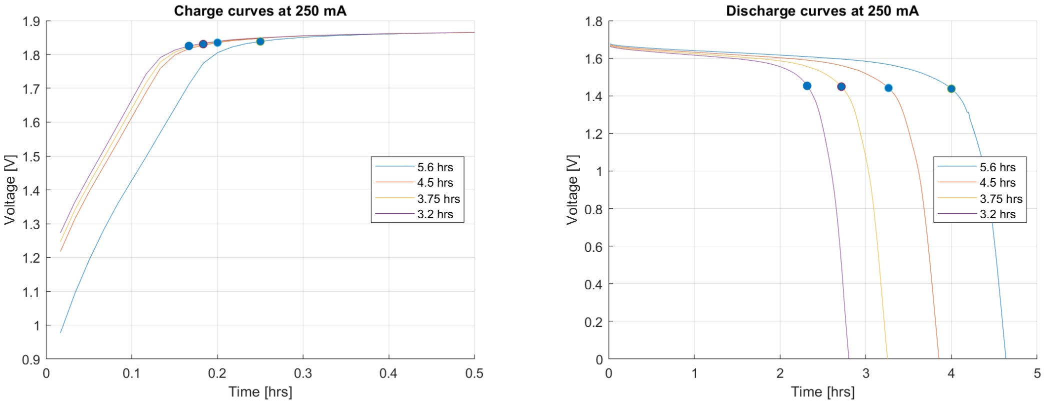

(a) The first 0.5 hrs of all measurements at 250 mA. Note the difference in initial voltage between the first and subsequent measurements.

(b) Discharge curves of all measurements at 250 mA. Apart from the elapsed discharge time and the slight differences in initial voltage, there are no other deviations that reflect the differences between the first and subsequent measurements.

Figure 24: Charge and discharge curves at 250 mA. The MVTPs for the charge and discharge phases are marked by the blue dot.

At all applied currents except 200 mA, the initial voltage of the first charge phase varies greatly from the other at the same applied current. The subsequent measurements are nearly indistinguishable, except for the total elapsed time. Figure 24 shows an example of this at 250 mA. This does not seem to have an influence on the subsequent discharge phases, as differences in initial voltage are almost negligible

(1 2% difference), and otherwise show similar behaviour.

5.2 Voltage-Time

For all charging phases, the voltages for the maximum voltage-time points correlate to the applied current levels. At lower currents, the voltage at the MVTP are slightly lower (just over 1.7 V at 50 mA), while the voltage is higher at higher currents (1.85 V at 300 mA). When discharging, the MVTP voltage hovers around 1.57 V from 50 mA up to 200 mA. At 250 mA and 300 mA however, the MVTP voltage drops significantly, down to 1.44 V and 1.39 V respectively. Upon closer look, another trend can be found in some measurement sets; during all except the 200 mA charging phases, the MVTP voltage decreases with each measurement (between 0.01 V and 0.015 V in total). During the discharge phases, there is some deviation between each measurement as well, albeit not as consistently as in the charging phases.

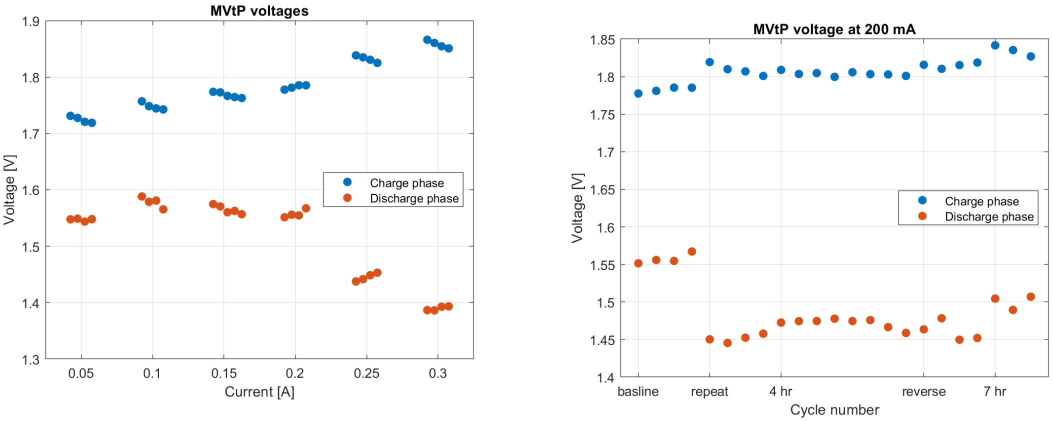

(a) The MVTP voltages at each applied current. The data points per applied current level are in chronological order. Note the decrease in MVTP voltage per subsequent cycle when charging.

(b) MVTP voltages for the repeat measurements at 200 mA. The x-axis marks the first measurement of the labeled set. Note the large decline from the initial measurement to the first set of repeat measurements.

Figure 25: An overview of the MVTP voltages. The values from the in-house cycling measurements follow the same trends as the results from BT1.

Figure 25 shows the MVTP voltages for the repeated measurements, both for the charging and discharging phases. Both when charging and discharging, the MVTP voltage takes on a variety of different values, ranging from 1.57 V down to 1.45 V when discharging, and from 1.78 V to 1.84 V when charging. With the points in the graphs being in order in which the measurements took place, there seems to be no significant correlation between the order in which the measurements are done (longer cycles first vs. shorter cycles first), and the resulting MVTP voltage, apart from the initial set of measurements.

5.3 Capacity & Efficiency

Table 3 and 4 show the energy and Coulombic efficiencies for the primary measurements from full charge to full discharge, colour-coded from lowest to highest result. Coulombic effiency results show a clear trend. Applying higher currents to the battery increases Coulombic efficiency, from below 70% at 50 mA, to above 80% at 300 mA. Energy effiency results show a maximum at around 200 mA, with shorter charging times being favoured over longer charging times. The recommended charge/discharge cycle makes sense in this context, as the battery operates under favourable conditions at 200 mA, maximizing the amount of available energy and charge.

Table 3: Coulombic efficiencies for all experiments, expressed in percentages. The elapsed charge time is expressed in equivalent time for 200 mA. The actual charge times can be found in table 2. Note the increase in efficiency with increasing current and decreasing charging time.

	50 mA	100 mA	150 mA	200 mA	250 mA	300 mA
7 hrs	58.87	72.14	77.86	80.02	82.83	83.85
5.6 hrs	63.23	75.60	81.06	83.31	85.65	86.61
4.7 hrs	67.71	78.43	82.51	85.86	86.77	88.33
4 hrs	69.54	79.89	84.09	87.30	87.61	88.73

Table 4: Energy efficiencies for all measurement, expressed in percentage points. There is a maximum at 4 hours of charging at 200 mA.

	50 mA	100 mA	150 mA	200 mA	250 mA	300 mA
7 hrs	52.04	63.90	67.94	69.78	67.20	65.13
5.6 hrs	56.14	66.84	70.34	71.93	68.88	67.20
4.7 hrs	59.67	68.81	71.15	73.93	69.50	68.11
4 hrs	61.03	69.74	71.98	74.60	69.90	68.26

These results are also reflected in the total amount of discharged energy for each applied current; at lower applied currents (50 mA to 150 mA), the amount of discharged energy is remarkably lower than at higher applied currents (200 mA to 300 mA). At 50 mA in particular, only 1.29 Wh was discharged, while at all other currents, around 1.7 Wh was discharged.

The repeat measurements at 200 mA yields a scale of different results, as shown in Figure 26. The first of these measurements (200 mA, from 7 hrs to 4 hrs charging time) show a similar energy and even improved Coulombic efficiency, while the repeats at 4 hrs are consistent at 70% energy and around 85% Coulombic efficiency respectively. The reverse order repeat measurement (200 mA, 4 hrs to 7 hrs charging time), however, see energy efficiency decline quickly (down to 65%), despite Coulombic efficiency remaining relatively unchanged. The set of eight repeated measurements at 200 mA, 4 hrs charging time show consistent performance at 85%

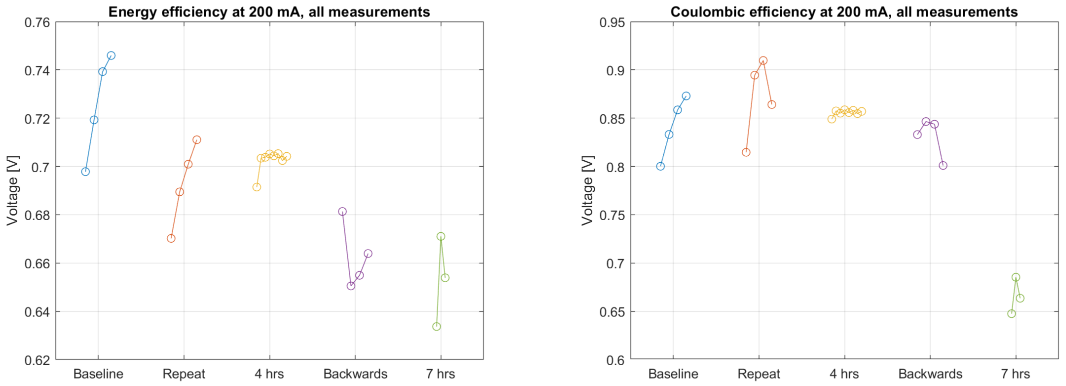

(a) The energy efficiency over repeated cycles at 200 mA.

(b) The Coulombic efficiency over repeated cycles at 200 mA.

Figure 26: The energy and Coulombic efficiencies at 200 mA throughout the repeated measurements.

Coulombic and 70% energy efficiency throughout. However, the final set of cycles at 7 hours charging again shows a decline in performance, with an average Coulombic and energy efficiency of 66% and 65% respectively.

Comparing the results to the data sets casts some doubt over the original data. A peak performance of 87 % Coulombic and 74.6 % energy efficiency, while decent, are lower than the results from the data sets, in which a consistent minimum of 95% Coulombic efficiency and 85% energy efficiency were seen. This raises the question whether this is due to equipment, the battery itself, or the cycling protocols (despite the fact that the most favourable result came directly from the cycling protocol that was recommended).

5.4 Constant Voltage Cycling

Three constant voltage measurements were performed on the battery to identify the total capacity. Considering the behaviour of a normal battery, its voltage rises as the SoC increases, followed by a region where the voltage remains near-constant. As the SoC approaches 1, the voltage spikes, indicating that the battery is fully saturated. In this case, a constant voltage measurement would see the current drop sharply, followed by a steady state region in which the current remains constant, then drop further to zero as the voltage of the battery exceeds the voltage of the measuring equipment.

The sea salt battery however, similar to the flow batteries, defies this trend. As shown in Figure 27, as the measurement proceeds through time, the current does not drop to 0, but instead tapers off to a steady state level. It does so over the time span of several days. While the initial fall in current takes the same amount of time for each measurement, the rate of subsequent decay differs between each measurement, with the first measurement decaying the quickest, and the last measurement

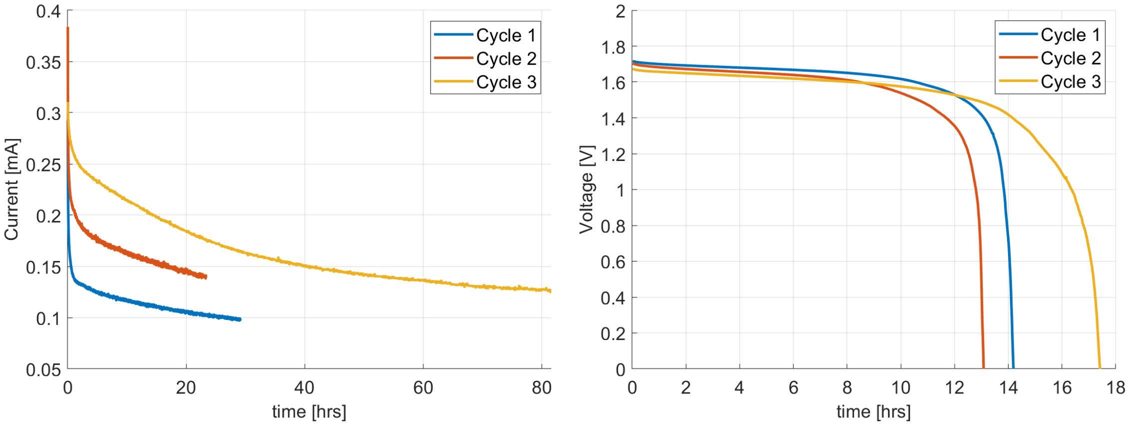

(a) Constant voltage charge curves. The current, despite dropping over time, did not reach 0 A, causing the charge phase to have to be ended manually. Note the increase in initial current with each following charge phase.

(b) Discharge phases for the constant voltage charge measurements. Note that these were performed under constant current. The duration of the charge phase does correlate loosely to the duration of the discharge phase.

Figure 27

decaying the slowest. The approximate value it trends towards differs too in each measurement; the first cycle ends the lowest at 100 mA, while the second and third cycle both seem to trend towards 120 mA, though over different time spans.

The extent to which the charge phase was allowed to continue also did not correlate strongly with the total discharge time. While the cycle with the longer charge phase also took longer to discharge, the difference in duration was not nearly as great as the difference between charge phase durations. The longer charge phase does seem to alter the physical processes somewhat, as the cycle with the longest charge phase sees a change in the discharge behaviour towards lower SoC values. Instead of the sharp drop in voltage, it seems to decrease over a longer period of time, without the more sudden onsets of the previous two cycles or any of the other measurements.

These findings seem to indicate that while the battery may have a stated capacity, the constant voltage charging method for determining the capacity does not work for this battery. Most likely there is some form of side-reaction taking place inside the battery that absorbs all the power once the battery approaches full capacity, which furthermore happens to have the same energy barrier that the electrical conversion of the active species has. The change in the discharge curve may indicate that the ideal amount of energy stored lies somewhere between cycles 2 and 3. Assuming this is the case, this raises two questions beyond the scope of this thesis. Firstly, how can we detect when the reaction that actually charges the battery ends, and the parasitic reaction takes over? Secondly, is this reaction reversible, and does the presence of whatever products this reaction produces interfere with the performance of the battery?

5.5 Voltage-Limited Constant Current Cycling

To see if V_{MVTP} would constitute a good approximate cut-off voltage when discharging, the battery was cycled multiple times between 1.87 V and 1.45 V. The results of these measurements can be seen in Figure 28.

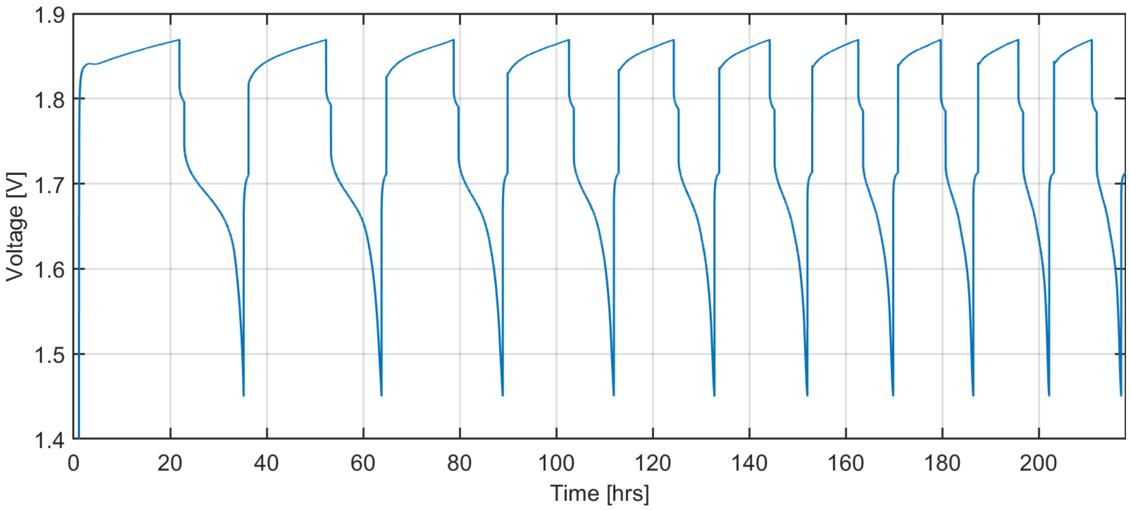

(a) The full measurement graph. Each cycle takes less and less time.

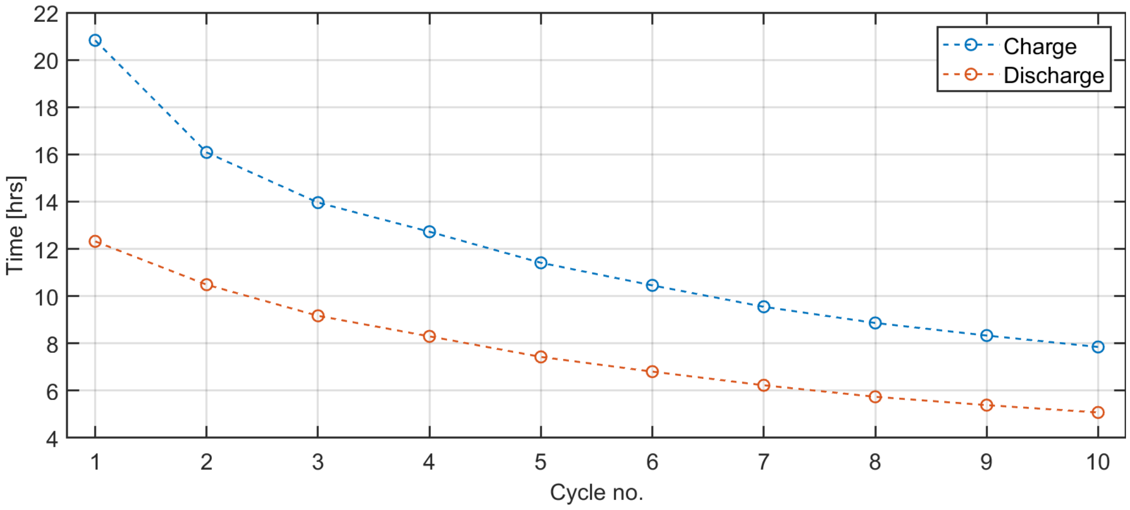

(b) Total charge and discharge times for each cycle, when cycled between 1.45 V and 1.87 V.

Figure 28: The full measurement for the repeated charge/discharge cycles between 1.45 V and 1.87 V. Each subsequent cycle is able to charge and discharge less current and energy.

The transient phase while charging has disappeared completely, with the voltage immediately jumping to around 1.82 V upon applying the charge current. This value increases over time, indicating that there is an accumulation of charge throughout these cycles. This is also reflected by the total duration of each charge phase, showing a gradual but steady decay as the cycles progress. The 1 hour rest period after each charge phase and discharge phase does not seem to be sufficient time to bring

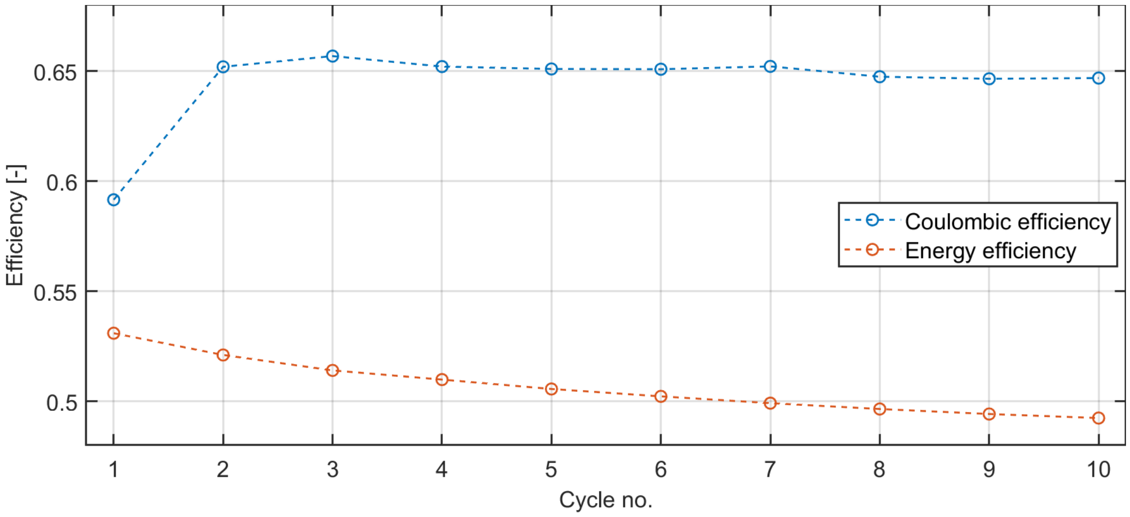

Figure 29: Coulombic and energy efficiencies of the voltage-limited constant current cycles. There is a large spike in Coulombic efficiency, as the first measurement had the battery charged from being (near) fully depleted. The subsequent charge phases start at higher voltages, thus take less time to hit the 1.87 V cut-off.

the concentrations inside the electrolyte back into equilibrium. This, combined with the results from the full discharges to 0 V, may mean that significant capacity is left unused after discharging. However, this conflicts with the Coulombic efficiency numbers, which show the lowest values at lower currents. More insight in the consistency of the electrolyte, both its composition and how the composition changes over time, is needed.

5.6 Single Cell Measurements

Four separate cells were also cycled using the recommended cycle (7 hours of charging, discharging to 0 V), with an added rest after charging, and an added rest after discharging. This was repeated 10 times. The results of these measurements can be seen in Figure 30.

There is some variation in the total length of the measurements for each cell. Cells 1 and 2 show the largest deviation in length, as well as the largest deviation in behaviour from the full battery. Cell 2 shows a more pronounced increase in voltage throughout each charging phase than the full battery, while the measurements on Cell 1 show interference towards later cycles, as well as showing a similar increased rise in voltage when charging towards later cycles. It is impossible to say for certain whether the error is due to battery failure or equipment failure, but it does put into question the robustness and reliability of the battery.

Figure 31 shows the Coulombic efficiencies of each cycle, for each cell. All cells perform similarly, with a consistent spread between one another. The only outlier is Cell 1, the efficiencies of which fall rather sharply in tandem with the introduction of the voltage interference. Of interest is how the efficiency seems

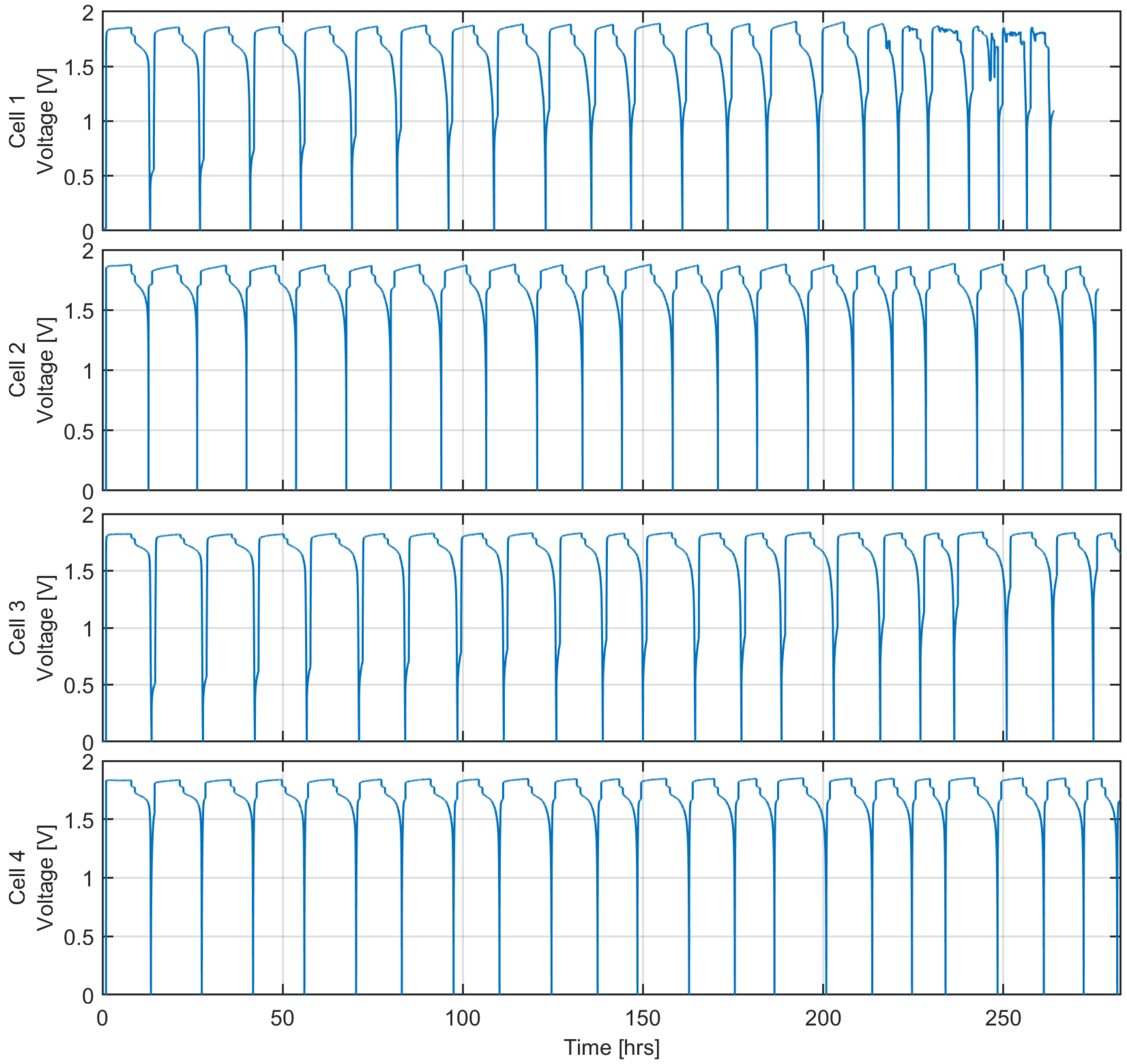

Figure 30: Cycling graphs for 4 separate cells

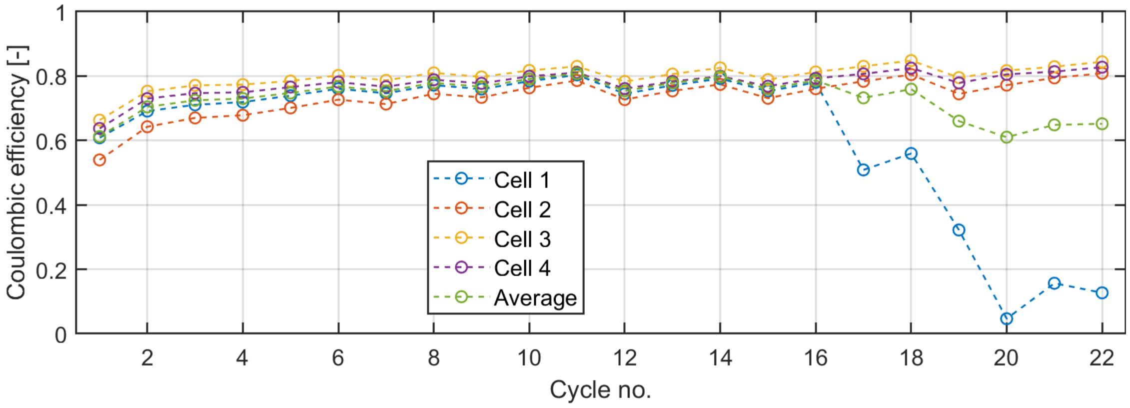

Figure 31: The Coulombic efficiencies per cycle for each cell. All cells perform similarly, except for Cell 1.

to increase with each cycle, making it seem as if the cells require pre-stressing to perform optimally. The average efficiency reflects the aberrant behaviour of Cel 1, with the efficiency increasing up to 16 cycles, then suddenly decreasing. This is in line with the Coulombic efficiency numbers of the battery at 200 mA, with the Coulombic efficiencies staying relatively consistent, until the very last set of measurements (as seen earlier in Figure 26).

5.7 Structural Integrity

Upon performing the cycling measurements, the battery underwent noticeable changes in colour and structure. There was a shift in colour, as shown in Figure 32; the battery in its untouched state is a dark green, almost black colour. After the measurements, however, its colour shifted, becoming a more yellow-greenish colour. The particular shade is reminiscent of different chlorine-based compounds like sodium hypochlorite or hydrogen chloride. The shift in colour does not seem to reverse upon discharging; it increases slightly in intensity and does not seem to fade upon discharging.

Furthermore, there seems to be a build-up of gaseous components in the cells of the battery. The battery has undergone visual changes, showing a slight bloating, with increased tension on the tape that is holding the cells together. It also feels more compressible, although no sloshing noises can be heard when agitating or shaking the battery. This, combined with the change in colour and findings in literature, leads us to believe there to be a build-up of Cl_2. Kim et al. [27] found similar a build-up of Cl_2 in the initial charging phase, though it was limited to the initial charging phase only. Though beyond the scope of this project, taking a sample of the electrolyte for analysis after repeated cycling might provide many answers to the internal workings.

(a) The front side of a new sea-salt cell. (b) The back side of a new sea-salt cell. (c) Two sea-salt cells after repeated cycling.

Figure 32: Sea-salt cells before and after repeated cycling. While not noticeable on the back side, the front side has shifted in colour, from nearly black to a lighter shade of ochre.

Considering the efficiencies measured from the separate cells and the battery pack as a whole, one could doubt the robustness of the cells. Considering that we saw a similar drop in efficiency towards later cycles, it could be that one of the cells in the battery already started to see the same degradation that was visible in Cell 1. Between 8 cells, having 2 fail is discouraging. One would hope that if significant money was used to purchase a larger bank of these batteries, a good majority would be fully functional. Assuming the battery does have a rapidly degradating cell, a 25% failure rate would be concerning.

Finally, there is one limitation throughout this whole series of measurements. All these measurements were performed on the same battery pack, and while the battery had ample time to rest in between measurements (sometimes up to several days), there was no way of knowing with certainty whether the battery was returned to the same state upon discharging, apart from the voltage of the battery. Better care could, and should, have been taken to make sure that the voltage was the same at the start of each measurement, to limit knock-on effects from previous measurements.

5.8 Modelling

This Section will detail the fitting of the DiBu-model to the in-house measurements.

The decision was made to only find the model constants for measurements at 200 mA. Considering the variation in performance between different measurements, even when using the same current, a comprehensive model would be beyond the scope of this project. An overview of all the calculated constants can be found in Tables 6, 5, 7 and 8. The highest and lowest fitted values are coloured red and blue respectively. When fitting the charge and discharge curves, a choice must be made whether to minimize the error in voltage, the error in energy capacity, or find a balance between both. As such, constants α, δ and σ have been fitted to minimize the voltage error (labeled 'dV'), the energy error (labeled 'dE'), and a combination of both (labeled 'average').

The equation used to model the recovery phase after discharging was able to match the results closely, as shown in Figure 33. However, just from the 200 mA results, neither constants are clearly defined. Constant β varies between 1.83 and 2.5, while γ values range from 1873 s up to 5951 s. The fitting is made easier since battery capacity does not factor into the equations. Therefore it is not necessary to balance the optimisation between minimising voltage error and capacity error, and can instead the optimisation be focused on fitting the voltage as closely as possible.

Figure 34 shows an example of fitting Equation 3 to the measurements. The solution seems to fit both the voltage curve and energy curve relatively well, although towards the end of the measurement, the voltage does accrue a large error. This is also seen in the energy availability fitting, as the measured capacity approaches

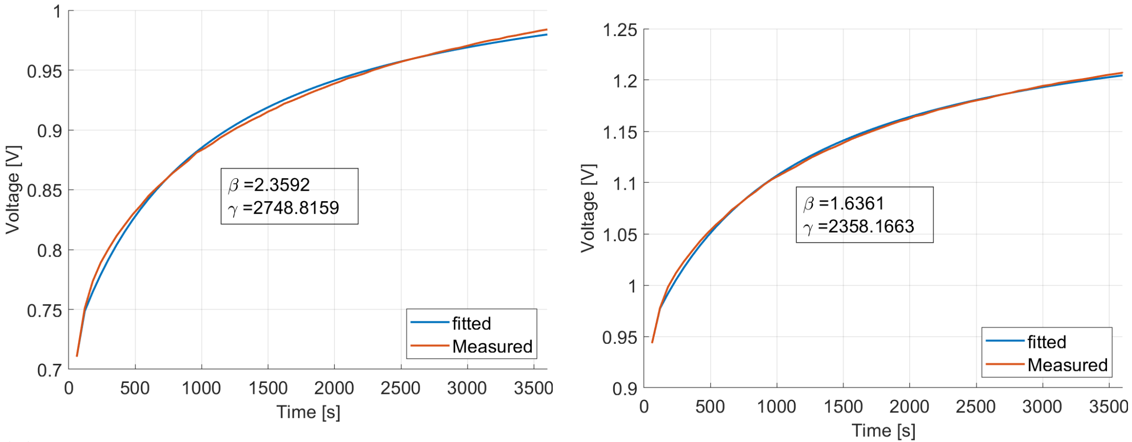

(a) Equation 8 manages to capture the voltage behaviour very closely.

(b) Similar to

Figure 33: Equation 8 yields the best-fitting results. While β does not vary strongly in value, γ does differ up to 10% between measurements.

0, the model starts to deviate in varying directions, depending on whether it is optimizing for voltage or energy. It is clear that the model breaks down towards lower energy capacity values and voltages.

Curve-fitting for the charge phase following Equations 5 and 6, while feasible from an energy standpoint, causes severe mismatches in the voltage; the Equations proposed by the authors do not account for the initial transient in voltage, instead only modelling the period in the charge phase after the initial increase has died down. As such, one could pick any arbitrary point on the charge curve to fit the model to, and find a different answer. The decision was made to model the charge phase starting from the MVTP of the respective charge phase, the results of which are shown in Figure 35.

From Figure 35, it is clear that despite Homan's adjustment [13] to fit the sea-salt battery better, his original Equation to model the charge phase is superior, both in in terms of voltage and the maximum deviation in energy capacity. However, that does not take away the fact that there is a large spread in calculated values, as shown in Table 8. With calculated values for constant σ ranging from 10.76 μV/A up to 18.00 μV/A, and constant δ ranging from 2.902 V/A up to 6.428 V/A, the question is how sensitive the outcome of each modelling phase is to the range of values of each constant.

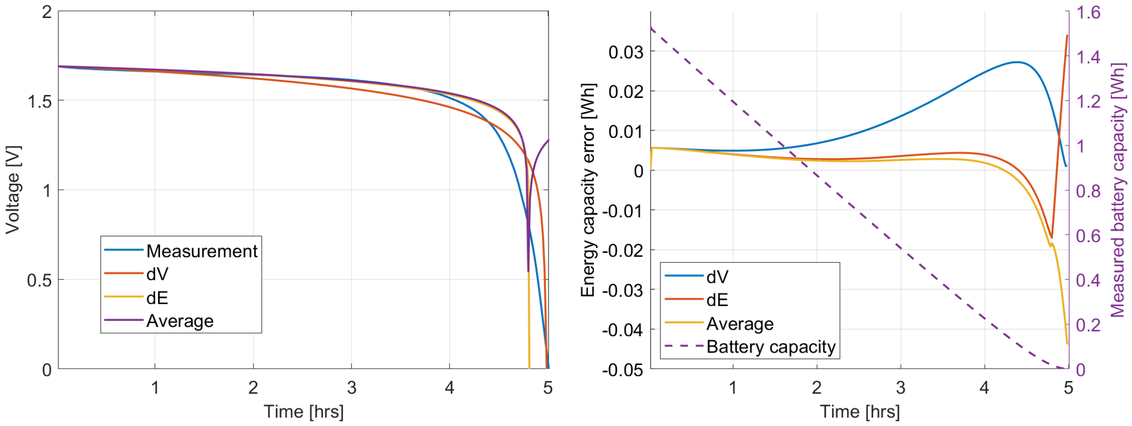

(a) While following the voltage curve somewhat closely, towards the end of the discharge phase the voltage behaviour starts showing anomalies and larger deviations, especially when optimizing the constant to minimize the deviation in energy.

(b) Similar to the voltage behaviour, the energy deviation increases sharply towards the end of the discharge phase. This is in part due to the fact that the measured energy becomes very small, which magnifies any difference in energy as a fraction.

Figure 34: Fitting the equations that model the discharge curve show discouraging results towards the end of the charge phase.

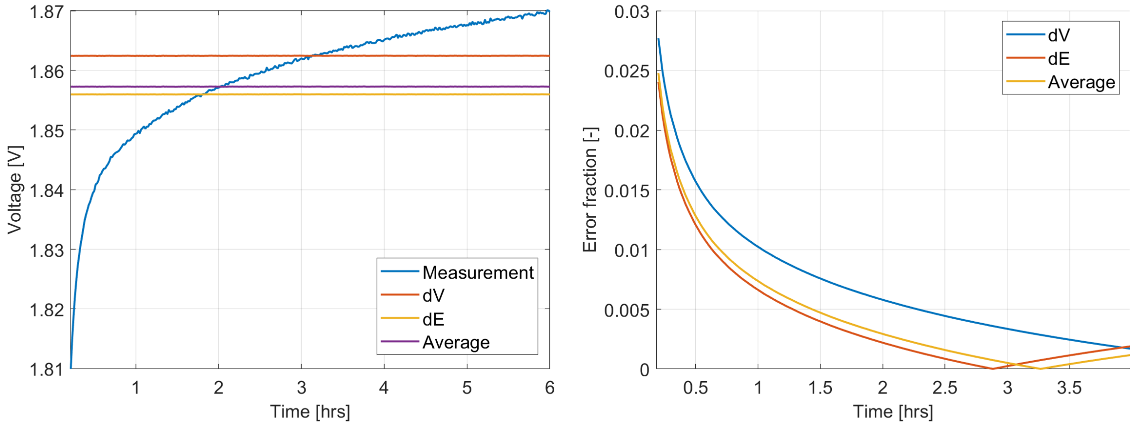

(a) Equation 6 offers a bad voltage fit overall.

(b) Equation 6 does perform decently in terms of energy modelling.

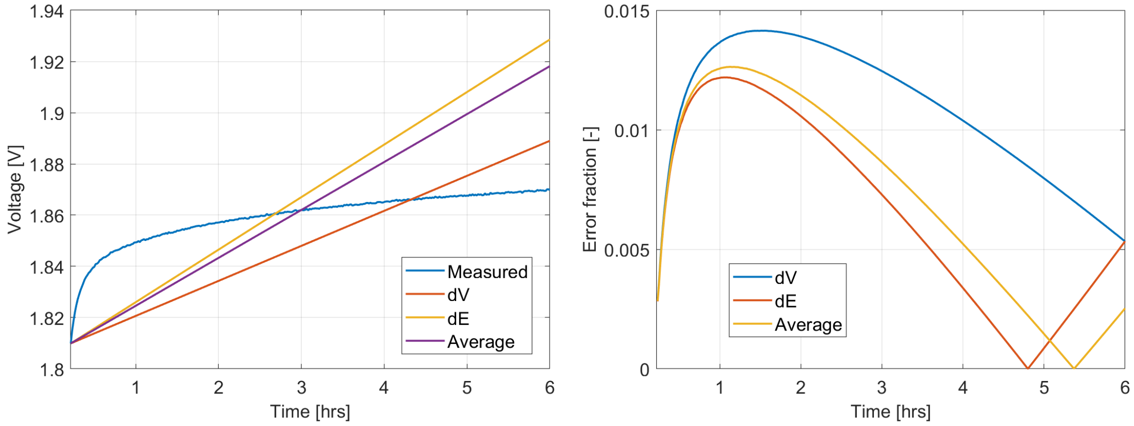

(c) Equation 5 too provides a mediocre voltage fit.

(d) The overall deviation in energy capacity is smaller when using Equation 5.

Figure 35: A comparison of the two different equations to model the charge phase. Even when only starting the model from the MVTP voltage and time, the deviation in voltage is considerable.

Table 5: Results for charge constant σ [μV/A]. There is a large spread in fitted values, from 10.76 μV/A up to 18.00 μV/A.

	Baseline			Repeat			4 hr Repeats			Reverse		
	Highest	Lowest	Average	Highest	Lowest	Average	Highest	Lowest	Average	Highest	Lowest	Average
dV	14.90	11.28	13.04	14.28	**10.76**	12.39	14.66	13.68	14.24	13.32	11.04	12.13
dE	18.00	13.20	15.59	17.38	12.24	14.57	**18.00**	16.68	17.38	16.16	12.58	14.29
Average	17.04	12.72	14.76	16.16	11.84	13.85	16.56	15.50	15.99	15.00	12.18	13.59

Table 6: Results for charge constant δ [A/V]. Again there is a large spread in values, from 2.9 A/V up to 6.5 A/V.

	Baseline			Repeat			4 hr Repeats			Reverse		
	Highest	Lowest	Average	Highest	Lowest	Average	Highest	Lowest	Average	Highest	Lowest	Average
dV	5.236	4.871	5.122	3.460	3.067	3.263	3.313	3.257	3.300	3.118	**2.902**	3.014
dE	**6.428**	5.724	6.088	3.913	3.314	3.632	3.731	3.683	3.711	3.462	3.192	3.311
Average	6.004	5.428	5.746	3.808	3.251	3.547	3.604	3.549	3.564	3.356	3.113	3.225

Table 7: Results for discharge constant α [μV/C]. There is an up to 50% difference between the lower and higher values.

	Baseline			Repeat			4 hr Repeats			Reverse		
	Highest	Lowest	Average	Highest	Lowest	Average	Highest	Lowest	Average	Highest	Lowest	Average
dV	58.90	14.00	31.40	31.70	31.00	31.40	54.90	51.50	53.28	58.90	50.20	50.85
dE	42.70	39.40	19.48	21.40	17.20	19.48	30.70	25.00	28.39	32.90	25.80	31.23
Average	45.40	40.30	19.28	20.90	17.20	19.28	29.50	26.90	28.55	33.10	29.30	32.15

Table 8: Results for post-discharge rest constants β [-] and γ [s]. Again there is a large spread in fitted values for each constant.

	Repeat			4 hr Repeats			Reverse		
	Highest	Lowest	Average	Highest	Lowest	Average	Highest	Lowest	Average
β	2.655	1.827	2.329	2.272	1.947	2.325	1.719	0.563	1.362
γ	5950.697	2748.816	3613.517	2749.470	2506.192	2641.369	3393.081	1859.553	2458.826

For both charge voltage approximations, the range of values found seem to fit the data reasonably well. Both the linear increase approximation and constant voltage approximation maintain an energy capacity error of below 3% in most cases, with most fits ranging between 2% and 3% energy capacity error. While the energy capacity model for the discharge curve performs decently well, the voltage prediction becomes highly problematic. Due to the nature of the equations, and depending on the value of the constants, the voltage can suddenly spike upwards, as the available energy in the battery goes below 0 Wh. This could cause major problems if applied in a broader energy system model.

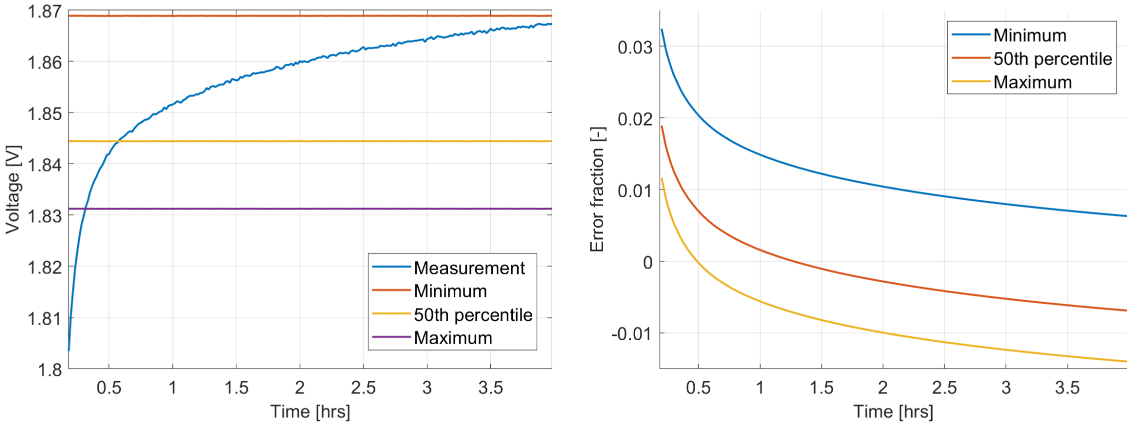

(a) The constant voltage approximation does not change much in quality as the value of constant σ varies.

(b) The constant voltage approximation creates a maximum energy capacity error of around 3%.

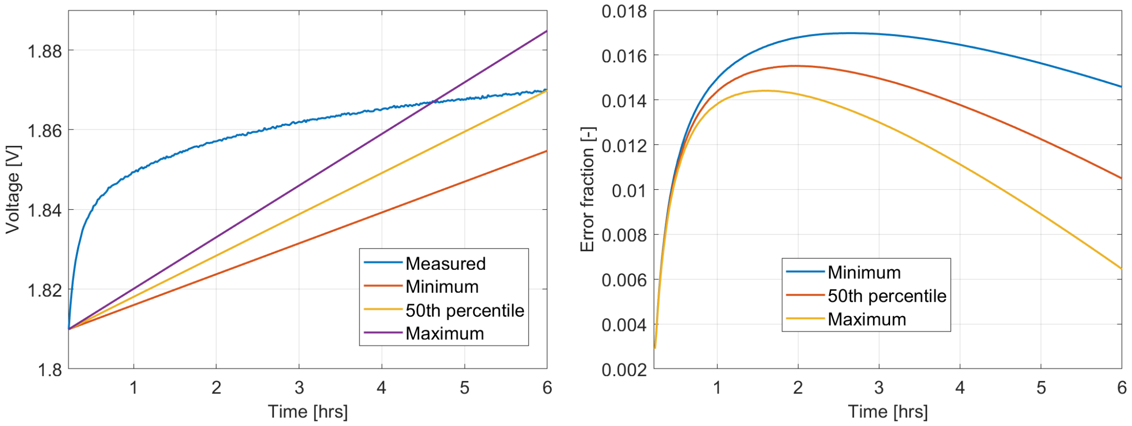

(c) The linear voltage increase approximation shows slightly more sensitivity.

(d) The linear voltage approximation still delivers decent performance in terms of energy estimation.

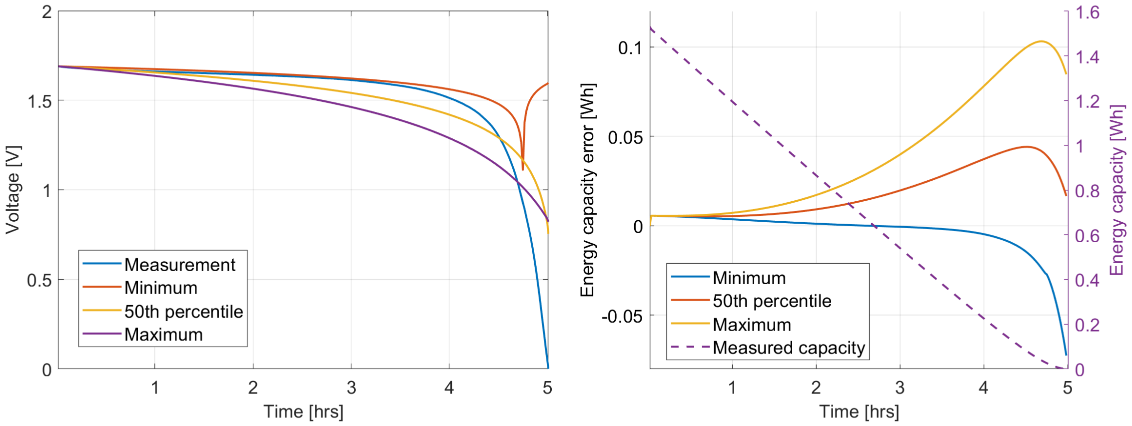

(e) The lower limits of the found constants for the discharge curve cause large deviations in voltage compared to measurements.

(f) Perhaps surprisingly, the large deviations in voltage still make for a relatively close approximation of the energy capacity of the battery.

Figure 36: Model equation results using the highest, middle, and lowest values found. The left column shows the voltage response of the Equations, the right column shows the error in energy capacity.

6 Conclusion

While the sea salt based battery does seem to be functional, the measurements so far seem to indicate that it may not be sufficient at providing the performance that is required. The rapidly diminishing performance casts serious doubts over its expected lifespan. The lack of a voltage increase towards the end of its charge cycle complicates the determination of the battery capacity, and it makes the battery more difficult to control by conventional BESS management systems. The battery also suffers from slow ion diffusion, as evidenced by the high voltage recovery after discharging at higher current levels. These two facts combined lead to an increased risk of overcharging, which may or may not be permanently damaging to the battery, as some of the observed changes in the structural integrity do not seem to reverse themselves after discharging. Modelling efforts seem to indicate Homan's model puts out decent energy capacity predictions, even if the voltage predictions are flawed. However, important steps are still missing, most importantly of which an accurate determination of the State of Charge, which is required to run the model optimally.

6.1 Research Questions

- *What is the energy and charge capacity of this sea-salt based battery?*
  In this work, the battery was charged up to 2.6 Wh, 1.40 Ah, with a maximum of 1.9 Wh, 1.15 Ah, discharged. However, with the constant voltage measurement being inconclusive, it is as of yet unknown what the real energy and charge capacity of the battery are.

- *What is the round-trip efficiency of the battery?*
  The highest coulombic efficiency measured was at 300 mA, 2.6 hours charge time, for an efficiency of 88.7%. The highest energy efficiency was measured at 200 mA, 4 hours charge time, for an efficiency of 74.6%. From the initial set of measurements, the recommended cycle seems a sufficient trade-off between efficiency and utilized capacity. However, repeat measurements show a decline in both coulombic and energy efficiency.

- *How do different cycling parameters influence performance?*
  Lower current values are discouraged. The battery showed the lowest performance at 50 mA, both in terms of efficiency and capacity. The battery shows an improvement in coulombic efficiency with increasing current. However, the energy efficiency peaks at 200 mA, then drops back down at higher current levels. Temperature effects were not evaluated in this work.

- *What are the set points to be used for safely charging and discharging the battery?*
  The MVTP voltage levels are a first approximation for a possible lower limit when discharging the battery. Dr. Ten's recommendation, however, is to fully discharge the battery to 0 V. This is in conflict with common battery

technologies, which all have a cut-off voltage at some level to protect the battery's internal structure and composition. A set of repeat measurements between 1.5 V and 1.8 V have shown to be well within safe operating limits, though the amount of energy that can be charged and discharged does decrease with each cycle.

- *Does the battery operate consistently enough to create a usable model?* The battery seems to operate consistently enough to at least have each of its phases (charge, post-charge rest, discharge, post-discharge rest) modelled using Homan's DiBu-model. However, the model itself may be fatally flawed, as it does not take into consideration the transient phase when charging, and its prediction for the voltage while discharging becomes unstable at lower charge capacities.

6.2 Recommendations

As with any body of work, there are several ways in which it can be improved. First, several different cut-off voltages should be evaluated for both the charge and discharge step. This should improve the lifespan of the battery, as well as enable the user to utilize its capacity to the fullest without reservations.

If full charge and discharge cycles are to be performed, a protocol should be made to ensure that the following charge phase starts with a fully drained battery. The results from our measurements show that especially at higher current levels, the battery was not fully discharged, despite the cut-off voltage having been set at 0 V. Possibly a rest period, followed by a slower secondary discharge could ensure a full discharge before the next measurement. Considerations should be made however, that this could possibly damage the battery over time.

Other methods to measure or otherwise evaluate the battery's efficiency and total capacity should be considered. Without a full understanding of the internal electro-chemical reactions and the battery's composition, the capacity remains impossible to calculate. Charge cycles with longer durations than the ones performed in this work could be considered, to see if there is a limit to how much charge and energy can be discharged from the battery.

It would be recommendable that destructive tests are performed. Exploring the upper limits of the battery could help to determine safe operating limits, and electrolyte sampling from both new and used batteries at various SoC levels could tell us more about whatever reactions are taking place, and determine the possible existence of irreversible parasitic side reactions that may hinder the battery's performance.

The modelling of the battery could be expanded. The DiBu-model could be applied more thoroughly, running full measurements to see if the model holds up over longer periods of time, and other models should be considered to model the behaviour of the battery, to capture the transient phase when charging, as well as to find a more robust way to capture the transient phase when discharging.

References

[1] NOAA, *NOAA National Centers for Environmental Information, State of the Climate: Monthly Global Climate Report for Annual 2021, published online January 2022*, 2022. [Online]. Available: `https://www.ncei.noaa.gov/access/monitoring/monthly-report/global/202113`.

[2] UNCED, "The United Nations Conference on Environment and Development," Tech. Rep., 1993. DOI: `10.1080/10464883.1993.10734558`.

[3] UNFCCC, "United Nations Framework on Climate Change Kyoto Protocol," Tech. Rep., 1997.

[4] European Commission, "EU emissions trading scheme," *EM: Air and Waste Management Association's Magazine for Environmental Managers*, no. FEB. Pp. 10–11, 2008, ISSN: 10889981. [Online]. Available: `https://climate.ec.europa.eu/eu-action/eu-emissions-trading-system-eu-ets_en`.

[5] Kamer van Koophandel, *Subsidies en regelingen voor verduurzaming @ www.kvk.nl.* [Online]. Available: `https://www.kvk.nl/advies-en-informatie/innovatie/duurzaam-ondernemen/subsidies-en-regelingen-voor-vergroening/`.

[6] Rijksoverheid, *Hoe lang kan ik nog koken op gas @ www.rijksoverheid.nl.* [Online]. Available: `https://www.rijksoverheid.nl/onderwerpen/duurzame-energie/vraag-en-antwoord/hoe-lang-kan-ik-nog-koken-op-gas` (visited on 11/21/2022).

[7] CBS, *Renewable electricity; production and capacity @ www.cbs.nl*, 2022. [Online]. Available: `https://www.cbs.nl/en-gb/figures/detail/82610ENG` (visited on 09/20/2022).

[8] ——, *Green electricity production up by 40 percent @ www.cbs.nl*, 2021. [Online]. Available: `https://www.cbs.nl/en-gb/news/2021/08/green-electricity-production-up-by-40-percent` (visited on 09/20/2022).

[9] Liander, *Beschikbaarheid capaciteit @ www.liander.nl*, 2022. [Online]. Available: `https://www.liander.nl/grootzakelijk/transportschaarste/beschikbaarheid-capaciteit` (visited on 09/20/2022).

[10] TenneT, *Voorlopige stop voor nieuwe grootverbruikers van elektriciteit noord-brabant en limburg @ www.tennet.eu*, 2022. [Online]. Available: `https://www.tennet.eu/nl/nieuws/voorlopige-stop-voor-nieuwe-grootverbruikers-van-elektriciteit-noord-brabant-en-limburg` (visited on 09/20/2022).

[11] A. Mittal, A. Rajput, K. Johar, and R. Kandari, *Microgrids, their types, and applications.* INC, 2022, pp. 3–40, ISBN: 9780323854634. DOI: `10.1016/b978-0-323-85463-4.00008-3`. [Online]. Available: `http://dx.doi.org/10.1016/B978-0-323-85463-4.00008-3`.

[12] A. Hirsch, Y. Parag, and J. Guerrero, "Microgrids: A review of technologies, key drivers, and outstanding issues," *Renewable and Sustainable Energy Reviews*, vol. 90, no. September 2017, pp. 402–411, 2018, ISSN: 18790690. DOI:

10.1016/j.rser.2018.03.040. [Online]. Available: `https://doi.org/10.1016/j.rser.2018.03.040`.

[13] B. Homan, "Batteries in Smart Microgrids," Ph.D. dissertation, University of Twente, 2020, ISBN: 9789036549578.

[14] B. Sundén, "Battery technologies," *Hydrogen, Batteries and Fuel Cells*, pp. 57–79, 2019. DOI: `10.1016/b978-0-12-816950-6.00004-x`.

[15] EEMB, "Lithium-Ion Battery LIR18650 2600mAh Datasheet," Tech. Rep., 2003. [Online]. Available: `https://www.ineltro.ch/media/downloads/SAAItem/45/45958/36e3e7f3-2049-4adb-a2a7-79c654d92915.pdf`.

[16] D. J. Garole, R. Hossain, V. J. Garole, V. Sahajwalla, J. Nerkar, and D. P. Dubal, "Recycle, Recover and Repurpose Strategy of Spent Li-ion Batteries and Catalysts: Current Status and Future Opportunities," *ChemSusChem*, vol. 13, no. 12, pp. 3079–3100, 2020, ISSN: 1864564X. DOI: `10.1002/cssc.201903213`.

[17] P. Keil and A. Jossen, "Charging protocols for lithium-ion batteries and their impact on cycle life-An experimental study with different 18650 high-power cells," *Journal of Energy Storage*, vol. 6, pp. 125–141, 2016, ISSN: 2352152X. DOI: `10.1016/j.est.2016.02.005`. [Online]. Available: `http://dx.doi.org/10.1016/j.est.2016.02.005`.

[18] P. Kurzweil, *Lithium Battery Energy Storage: State of the Art Including Lithium-Air and Lithium-Sulfur Systems.* Elsevier B.V., 2015, pp. 269–307, ISBN: 9780444626103. DOI: `10.1016/B978-0-444-62616-5.00016-4`. [Online]. Available: `http://dx.doi.org/10.1016/B978-0-444-62616-5.00016-4`.

[19] R. Perez, "Lead-Acid Battery State of Charge vs. Voltage," *Home Power*, no. 36, pp. 66–70, 1993.

[20] D. A. Rand and P. T. Moseley, *Energy Storage with Lead-Acid Batteries.* Elsevier B.V., 2015, pp. 201–222, ISBN: 9780444626103. DOI: `10.1016/B978-0-444-62616-5.00013-9`. [Online]. Available: `http://dx.doi.org/10.1016/B978-0-444-62616-5.00013-9`.

[21] D. R. Wilburn, "Comparison of the U.S. Lead Recycling Industry in 1998 and 2011," Tech. Rep., 2014.

[22] Energizer, *Nickel Metal Hydride Batteries, Handbook and Application Manual*, 2018. [Online]. Available: `https://data.energizer.com/PDFs/nickelmetalhydride_appman.pdf`.

[23] P. Bernard and M. Lippert, *Nickel-Cadmium and Nickel-Metal hydride Battery Energy Storage.* Elsevier B.V., 2015, pp. 223–251, ISBN: 9780444626165. DOI: `10.1016/B978-0-444-62616-5.00014-0`. [Online]. Available: `http://dx.doi.org/10.1016/B978-0-444-62616-5.00014-0`.

[24] Z. Huang, G. Du, N. Wollongong, and B. Group, "Nickel-based batteries for medium- and large-scale energy storage," in *Advances in batteries for medium-*

and large-scale energy storage, vol. 1, 2015, ISBN: 9781782420132. DOI: `10.1016/B978-1-78242-013-2.00004-2`.

[25] O. Hasvold, H. Henriksen, E. Melvax, *et al.*, "Sea-water battery for subsea control systems," *Journal of Power Sources*, vol. 65, no. 1997, pp. 253–261, 2007.

[26] P. K. Shen and A. C. C. Tseung, "Development of an aluminium/sea water battery for sub- sea applications," *Journal of Power Sources*, vol. 47, pp. 119–127, 1994.

[27] J.-k. Kim, E. Lee, H. Kim, C. Johnson, and J. Cho, "Rechargeable Seawater Battery and Its Electrochemical Mechanism," *Chemelectrochem*, vol. 60439, pp. 328–332, 2015. DOI: `10.1002/celc.201402344`.

[28] S. T. Senthilkumar, M. Abirami, J. Kim, W. Go, S. Min, and Y. Kim, "Sodium-ion hybrid electrolyte battery for sustainable energy storage applications," *Journal of Power Sources*, vol. 341, pp. 404–410, 2017, ISSN: 0378-7753. DOI: `10.1016/j.jpowsour.2016.12.015`. [Online]. Available: `http://dx.doi.org/10.1016/j.jpowsour.2016.12.015`.

[29] Y. Zhang, J. S. Park, S. T. Senthilkumar, and Y. Kim, "A novel rechargeable hybrid Na-seawater flow battery using bifunctional electrocatalytic carbon sponge as cathode current collector," *Journal of Power Sources*, vol. 400, pp. 478–484, Oct. 2018, ISSN: 03787753. DOI: `10.1016/j.jpowsour.2018.08.044`.

[30] J. Han, S. Min, W. Go, S. T. Senthilkumar, D. Jeon, and Y. Kim, "Development of coin-type cell and engineering of its compartments for rechargeable seawater batteries," *Journal of Power Sources*, vol. 374, no. October 2017, pp. 24–30, 2018, ISSN: 0378-7753. DOI: `10.1016/j.jpowsour.2017.11.022`. [Online]. Available: `https://doi.org/10.1016/j.jpowsour.2017.11.022`.

[31] J. Park, J.-s. Park, S. T. Senthilkumar, and Y. Kim, "Hybridization of cathode electrochemistry in a rechargeable seawater battery : Toward performance enhancement," *Journal of Power Sources*, vol. 450, no. December 2019, p. 227 600, 2020, ISSN: 0378-7753. DOI: `10.1016/j.jpowsour.2019.227600`. [Online]. Available: `https://doi.org/10.1016/j.jpowsour.2019.227600`.

[32] L. Wei, L. Zeng, M. C. Wu, X. Z. Fan, and T. S. Zhao, "Seawater as an alternative to deionized water for electrolyte preparations in vanadium redox flow batteries," *Applied Energy*, vol. 251, no. November 2018, 2019. DOI: `10.1016/j.apenergy.2019.113344`.

[33] J. Yu, C.-x. Zhao, J.-n. Liu, B.-q. Li, C. Tang, and Q. Zhang, "Green Chemical Engineering Seawater-based electrolyte for Zinc – air batteries," *Green Chemical Engineering*, vol. 1, no. 2, pp. 117–123, 2020, ISSN: 2666-9528. DOI: `10.1016/j.gce.2020.09.013`. [Online]. Available: `https://doi.org/10.1016/j.gce.2020.09.013`.

[34] D. Lim, C. Dong, H. W. Kim, *et al.*, "Redox chemistry of advanced functional material for low-cost and environment-friendly seawater energy storage," *Materials Today Energy*, vol. 21, p. 100 805, 2021, ISSN: 2468-6069. DOI: `10.1016/j.mtener.2021.100805`. [Online]. Available: `https://doi.org/10.1016/j.mtener.2021.100805`.

[35] H.-s. Yang, M.-w. Park, K.-h. Kim, O. Lun, T.-i. Jeon, and J. Kang, "Facile in situ synthesis of dual-heteroatom-doped high-rate capability carbon anode for rechargeable seawater-batteries," *Carbon*, vol. 189, pp. 251–264, 2022, ISSN: 0008-6223. DOI: `10.1016/j.carbon.2021.12.066`. [Online]. Available: `https://doi.org/10.1016/j.carbon.2021.12.066`.

[36] C. J. Raj, R. Manikandan, M. Rajesh, *et al.*, "Cornhusk mesoporous activated carbon electrodes and seawater electrolyte : The sustainable sources for assembling retainable supercapacitor module," *Journal of Power Sources*, vol. 490, no. November 2020, p. 229 518, 2021, ISSN: 0378-7753. DOI: `10.1016/j.jpowsour.2021.229518`. [Online]. Available: `https://doi.org/10.1016/j.jpowsour.2021.229518`.

[37] P. Pourbeik, S. Soni, A. Gaikwad, and V. Chadliev, "Providing primary frequency response from photovoltaic power plants," vol. 12, pp. 5–12, Oct. 2018.